

Twenty-year monitoring of the surface magnetic field of peculiar stars

F. Leone¹, M. Giarrusso², M. Cecconi³, R. Cosentino³, M. Munari¹, A. Ghedina³,
F. Ambrosino⁴, W. Boschin^{3,5,6}

¹INAF - Osservatorio Astrofisico di Catania, Via S. Sofia 78, I-95123 Catania, Italy

²INFN - Laboratori Nazionali del Sud, Via S. Sofia 62, I-95123 Catania, Italy

³INAF - Fund. Galileo Galilei, Rambla José Ana Fernández Pérez 7, 38712 Breña Baja (La Palma), Canary Islands, Spain

⁴INAF - Osservatorio Astrofisico di Roma, Via Frascati 33, I-00078, Monteporzio Catone (Roma) Italy

⁵Instituto de Astrofísica de Canarias (IAC), Calle Vía Láctea s/n, 38205 La Laguna, TF - Spain

⁶Departamento de Astrofísica, Universidad de La Laguna (ULL), 38206 La Laguna, TF - Spain

Received To be inserted later, accepted To be inserted later

ABSTRACT

Magnetic chemically peculiar stars of the main sequence can present rotational periods as long as many decades. Here we report the results of an observational campaign started in 2001 aimed to establish these very long periods from the variability of the surface magnetic field, as measured from the Zeeman split of the FeII 6149.258 Å spectral line. Thirty-six stars have been monitored with several high-resolution spectrographs at different telescopes, for a total of 412 new collected spectra. To extend and fill at the best the time frame, we have also exploited all public archives containing high-resolution spectra, many not yet published. At the start of the campaign, most of the variability periods were unknown and stars selected for the sharpness of their spectral lines only, and thirteen stars were found to present variability periods on the scale of weeks. A final plot of magnetic field strength versus rotational periods is given.

Key words: Stars: magnetic fields, Stars: individual: HD 201601, Spectroscopy

1 INTRODUCTION

Since Babcock (1960) measurements of the surface magnetic field B_s (average over the stellar visible disk of the magnetic modulus) of the star HD 215441, massive measurements of B_s for Magnetic Chemically Peculiar (MCP) stars have been reported by Preston (1971), Mathys et al. (1997) (=M97) and Mathys (2017)(=M17). Nowadays, B_s can be straightly and accurately measured from the Zeeman split of the FeII 6149.258 Å spectral line, because of the only two Zeeman subcomponents π in a coincidence of two components σ (Mathys 1990).

In the framework of the oblique rotator model by Babcock (1949) and Stibbs (1950), MCP stars present photometric, spectroscopic, and magnetic variability with a single period as a consequence of the stellar rotation. The possibility to measure the rotational period from the FeII 6149.258 Å surface magnetic field modulation is probably the most reliable for very long-term variables. All the necessary information is coded in a single spectrum with no necessity of standard stars or zero-points as in the case of photometry.

This paper reports the results of an observational campaign started in 2001 to measure and monitor the surface field of 36 MCP stars whose rotational period was expected to be very long, even decades, because of the sharpness of their spectral lines.

Field measurements are from high-resolution spectroscopy of the FeII 6149.258 Å line. And, to extend, as much as possible, the time frame we have also explored all public astronomical archives and mined the literature. We have also analyzed some of our spectra dated back to 1995.

In Section 2, we present the: 1) operated high-resolution spectrographs, 2) reduction methods, 3) procedure to measure B_s from the FeII 6149.258 Å spectral line, and 4) method to establish the variability period. In Section 3, we present star-by-star the determined rotational periods. If possible, these periods have been checked or determined contextually to the effective magnetic field B_e (average over the stellar visible disk of the magnetic components along the line of sight) and/or photometric measurements. In the conclusions, we present the found relation between rotational periods and magnetic field strength.

2 OBSERVATIONS, ARCHIVES, DATA REDUCTION AND PERIOD SEARCH

We have carried out high-resolution spectroscopy of 36 MCP stars with the different instruments listed in Table 1, for a total of 412 new spectra. Data have been reduced by using IRAF routines as described in Leone et al. (2017). To extend as much as possible

Table 1. List of spectrographs used to measure the stellar surface magnetic fields. Spectral resolution R [k] = $\frac{\lambda}{\Delta\lambda}/1000$ is given. For any instrument, N is the number of B_s measurements from here acquired spectra. A two-letter identification is used for any instrument.

Spectrograph@Telescope	R [k]	N	Reference	
CAOS@OAC	CS	71	123	Leone et al. (2016)
HARPS@ESO 3.6m	HS	115	20	Mayor et al. (2003)
HARPS-N@TNG	HN	115	81	Cosentino et al. (2013)
UCLES@AAT	UC	120	22	Horton et al. (2012)
SARG@TNG	SG	≤ 164	53	Gratton et al. (2001)
CES@ESO 3.6m	CE	220	2	Enard (1982)

Table 2. Archives hosting high-resolution spectra of long period magnetic chemically peculiar stars. For any instrument, N is the number of B_s measurements from archive spectra.

Spectrograph@Telescope	R [k]	N	Reference	
ELODIE@OHP-1.9m	EE	40	6	Baranne et al. (1996)
FEROS@ESO-2.2m	FS	48	6	Kauffer et al. (1999)
EMMI@ESO-NTT	EM	60	2	D’Odorico (1990)
NES@BTA	NS	60	6	Panchuk et al. (2009)
ESPaDOns@CFHT	ES	65	85	Silvester et al. (2012)
NARVAL@TBL	NL	65	16	Silvester et al. (2012)
UCLES@AAT	UC	90	10	Horton et al. (2012)
UVES@ESO-UT2	US	100	72	Dekker et al. (2000)
HARPS@ESO-3.6m	HS	115	350	Mayor et al. (2003)
GECKO@CFHT	GO	120	21	Gaspey (1993)
CES@ESO-3.6m	CE	220	7	Enard (1982)

the time frame for determining the variability periods we have exploited all public archives storing high-resolution spectra (Table 2) with the FeII 6149.258 Å line. A total of 581 spectra have been retrieved.

Following Mathys (1990, 2017); Mathys et al. (1997), measurements of the surface magnetic fields B_s have been obtained from the wavelength distance $\Delta\lambda$ of Zeeman subcomponents of the FeII 6149.258 Å lines:

$$B_s[G] = 20974 \Delta\lambda [\text{Å}]$$

in the weak field approximation.

The wavelengths of Zeeman subcomponents have been obtained with a 2-gaussian fit (top panel of Figure 1). Error in a surface magnetic field measurement is from the propagation of errors in the determination of subcomponent positions. If a blend is present with the not yet identified spectral line at ~ 6148.84 Å a third gaussian component has been considered (bottom panel of Figure 1).

In this paper, the measurements of the surface magnetic field by Mathys et al. (1997) (=M97) and Mathys (2017) (=M17) are fundamental. The huge observational effort of these authors represents a significant enlargement of the time base for many stars. Whenever it was possible, we have retrieved the original spectroscopic data of these authors and obtained a measure of the surface magnetic field. In average, our measurements are 50 G smaller than Mathys values. For this reason, whenever the original spectra of Mathys and coworkers were not available, we have combined B_s values published by M97 and M17 with our values after this shift.

Variability periods are here determined from the Lomb-Scargle (Press & Rybicki 1989) periodogram of the surface magnetic field measurements: $LS(B_s)$. If necessary, the periodograms of other observables ($LS(O^i)$) have been also computed and the final

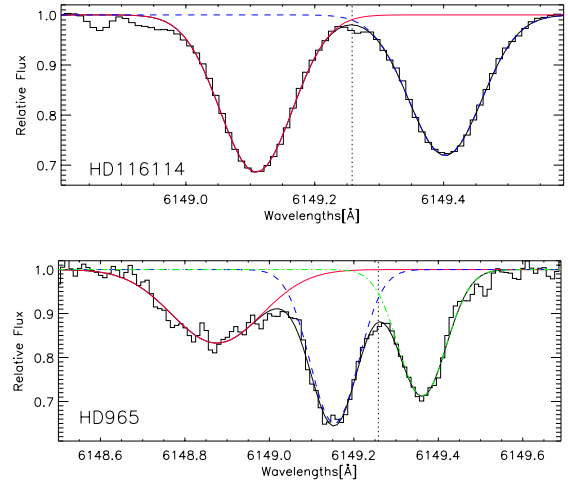


Figure 1. Distances of FeII 6149.258 Å line Zeeman components are from a 2-gaussian fit (a) and 3-gaussian fit including the still unidentified spectral line (b) at ~ 6148.84 Å.

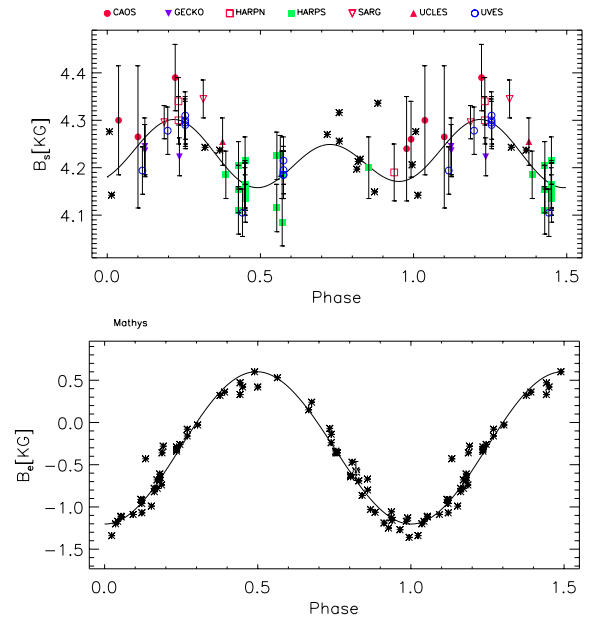


Figure 2. HD965. B_s and B_e variation.

period determined as the position of the highest peak in the product: $LS(B_s, O^1, O^2, \dots) = \frac{LS(B_s)}{LS^{max}(B_s)} \times \prod_i \frac{LS(O^i)}{LS^{max}(O^i)}$. We assume that spurious peaks in any periodogram due to data sampling and noise are not in coincidence and they cancel or mitigate in the product. Normalization of any periodogram to its maximum value is equivalent to assume the same weight to all datasets.

Uncertainty in period determination is always controversial and in the literature a large number of methods has been proposed to estimate the period error. In the present framework, the papers by Pyper & Adelman (2017) (=P17) and M17 are relevant for many of the here presented stars. Determining the periods with the Scargle method, P17 estimate its precision by “the practical method of comparing the two good data sets most widely separated in time and determined how much the period had to be changed to see a

Table 3. Observed stars and here adopted ephemeris for the B_s variability. The last column is used to state if the B_s and B_e variabilities are in phase as expected for a magnetic dipole.

HD / HDE	Literature Ephemeris		Reference	Here determined or adopted Ephemeris	
	JD = 240000+	Period (days)		JD = 240000+	Period (days)
965	$B_e^{\min} = 51000.0$	6030±200	Mathys et al. (2019b)	$B_e^{\min} = 51000.0$	6030
2453	$B_e^{\min} = 42213.0$ $c_1^{\max} = 48440.911$	521±2 518.2±0.5	Mathys (2017) Pyper & Adelman (2017)	$B_e^{\min} = 48440.911$	518.2
9996	$y^{\max} = 53016.610$ $B_e^{\min} = 33301.360$	7850±100 7936.522	Pyper & Adelman (2017) Bychkov et al. (2019)	$B_s^{\max} = 49200.0$	7850
12288	$B_e^{\max} = 48499.87$ $v^{\max} = 51131.772$ $v^{\max} = 57218.6$	34.9±0.2 34.99±0.01 35.73±0.2	Wade et al. (2000b) Pyper & Adelman (2017) Bernhard et al. (2020)	$B_e^{\max} = 51131.9$	34.993±0.003
14437	$v^{\max} = 57077.7$ $B_e^{\max} = 48473.846$	26.78±0.1 26.87±0.02	Bernhard et al. (2020) Wade et al. (2000b)	$v^{\max} = 49230.528$	26.734±0.007
18078	$B_s^{\max} = 49930.0$	1358±12	Pyper & Adelman (2017) Mathys et al. (2016a)	$B_s^{\max} = 49916$	1352±6
29578		>> 1800	Mathys (2017)	$B_s^{\max} = 51950.0$	4000/9230
47103		> 10	Wraight et al. (2012)	$B_s^{\max} = 50098.99$	17.683±0.004
50169		10600±300	Mathys et al. (2019a)	$B_s^{\max} = 41600.0$	10600±300
51684	$B_s^{\max} = 49947.0$	371±6	Mathys et al. (2019a)	$B_s^{\max} = 53617$	366±1
55719		>> 3650	Mathys (2017)	48500	≥ 14000
61468	$B_e^{\max} = 50058.5$	322±3	Mathys (2017)	$B_e^{\max} = 50058.5$	321±1
75445		6.291±0.002 ?	Mathys (2017)		> 5000
81009	$v^{\min} = 48646.878$ $v^{\max} = 44483.420$	33.987±0.002 33.984±0.055	Pyper & Adelman (2017) Wade et al. (2000c)	$B_s^{\max} = 48645.9$	33.987±0.002
93507	$B_e^{\min} = 49800.0$	556±22	Mathys et al. (1997)	$B_s^{\max} = 48965.0$	562±5
94660	$B_s^{\min} = 47000.0$	2800±200	Mathys (2017)	$B_s^{\max} = 48284.0$	2830±140
110066	phot. not variable $B_s^{\min} = 49826.738$	6.4769±0.0011	Pyper & Adelman (2017) Bychkov et al. (2020)		> 10 500
116114	$m^{\max} = 54352.057$ $B_e^{\max} = 47539.000$	5.3832 27.61	Wraight et al. (2012) Mathys (2017)	$B_s^{\max} = 40350.0$	> 17700
126515	$B_e^{\max} = 37015.000$ $v^{\min} = 52031.708$	129.95 129.95±0.02	Mathys (2017) Pyper & Adelman (2017)	$B_e^{\max} = 37015.0$	129.95
137949	many decades phot. not variable $B_e^{\max} = 38166$	5195	Landstreet et al. (2014) Pyper & Adelman (2017) Mathys (2017)		> 10 000
142070	$B_e^{\max} = 49878.2$	3.3718	Mathys (2017)	$B_e^{\max} = 49878.2$	3.3721±0.0002
144897	$B_e^{\max} = 49133.7$	48.57±0.15	Mathys (2017)	$B_e^{\max} = 491157.1$	48.60±0.02
150562		> 1600	Mathys (2017)	$B_e^{\max} = 54317.0$	2100±200
154708	$B_e^{\max} = 54257.740$	5.363±0.003	Landstreet et al. (2014)	$B_e^{\max} = 53662.57$	5.367±0.001
318107	$B_e^{\max} = 48800.000$	9.7088±0.0007	Bailey et al. (2011)	$B_e^{\max} = 48800.0$	9.7089±0.0002
165474		>>3300	Mathys (2017)	$B_e^{\max} = 52150.0$	≥ 9900
166473	$B_s^{\max} = 48660.0$	3836±30	Mathys et al. (2020)	$B_s^{\max} = 48660.0$	3836
177765		>>1800	Mathys (2017)		≥13500
178892	$v^{\max} = 52708.562$	8.2549	Semenko et al. (2011)	$B_s^{\max} = 52696.850$	8.2572±0.0016
187474	$B_e^{\min} = 46766.000$	2345	Mathys (2017)	$B_e^{\min} = 47870.0$	2329±60
188041	$v^{\min} = 49904.860$ $B_e^{\max} = 46319.5$	223.826±0.040 223.78±0.10	Pyper & Adelman (2017) Mathys (2017)	$B_e^{\max} = 49797.921$	223.826
192678	$B_e^{\max} = 44890.170$	6.4193±0.003	Pyper & Adelman (2017)	$B_s^{\max} = 49112.76$	6.4199±0.0001
335238	47000	48.7±0.1	Mathys (2017)	$B_e^{\max} = 57222.7$	48.985±0.007
201601	$B_e^{\min} = 52457.1$	35462.5±1149	Bychkov et al. (2016)	$B_e^{\max} = 52200.0$	90.49×365.25
208217	$B_e^{\max} = 47028.0$	8.44475±0.00011 8.317±0.001	Mathys (2017) David-Uraz et al. (2019)	$B_s^{\max} = 47027.094$	8.445±0.005
216018		> 10 >>2000	Wraight et al. (2012) Mathys (2017)	$B_e^{\max} = 49531.870$	34.044±0.007

definite shift in phase”. [Mathys et al. \(2019b\)](#) estimate the period uncertainty “by plotting a phase diagram of the measurements for a series of tentative values of the period around the one suggested by the periodogram, one can visually identify the period value that minimizes the phase shifts between field determinations from different rotation cycles, and constrain the range around that value for which those phase shifts remain reasonably small.” We prefer a clinical decision based on the σ value of a gaussian fit of the highest peak in the periodogram as uncertainty in the period determination. If the literature period is coincident within errors with the here determined value and the literature period has been determined with a smaller error, we have adopted the period of the literature.

3 SINGLE STARS

Table 3 lists the 36 MCP stars object of this paper and it reports the ephemeris from the literature and the here adopted ones. For any star, measured surface field values are listed from Table 4 to 39 with errors, Heliocentric Julian Date (HJD) and used spectrographs as coded in Tables 1 and 2. Field measurements by Mathys and coworkers are indicated with asterisks in the hereafter figures. If data from the literature are here used sources and symbols are given in the corresponding section and figure, respectively. Hereafter, if different photometric data sets of are available to better determine the variability period of a star, these are overplotted after an ad hoc shift

3.1 HD 965

[Mathys et al. \(2019b\)](#) found the B_s measurements of HD 965, collected between 1993 and 2008, do not show significant variations. Differently, these authors found the B_e measurements, collected between 1995 and 2017, variable with the period of 6030 ± 200 days.

We have obtained high-resolution spectra of HD 965 between 2001 and 2021, and retrieved spectra from the CFHT and ESO archives. The list of our B_s measurements of HD 965 is given in Table 4. There is no clear evidence of a periodically variable surface magnetic field: the average value is $B_s = 4240 \pm 70$ G, where the r.m.s. is comparable to the error of a single field measure. However, B_s measurements folded with [Mathys et al. \(2019b\)](#) period (Table 3) present a double wave variation and their fit suggest minima in coincidence with the extrema of the effective magnetic field, while B_s maxima are in coincidence with null values (Fig. 2). A magnetic field certainly does not dominated by the dipolar component.

3.2 HD 2453

Two periods have been almost simultaneously published to account for the HD 2453 variability: 1) 521 ± 2 days by M17 from B_e measurements and 2) 518.2 ± 0.5 day by P17 from Strömgren photometry.

Our B_s measurements of HD 2453 (Table 5) extend the 2700-day time coverage by M17 to 11000 days. But, with an average value of $B_s = 3690 \pm 60$ G and a scatter comparable to the error of a single field measure, it is not possible to ascertain a clear variability of the surface magnetic field. The single B_e measurement obtained by [Romanyuk et al. \(2016\)](#) on JD = 2 455 075.417 equal to $B_e = -1160 \pm 50$ G let the 518.2 day period be the most probable. The Lomb-Scargle analysis of B_e (by M17, [Wolff \(1975\)](#); [Romanyuk et al. \(2016\)](#)) and c_1 (by [Wolff \(1975\)](#); [Pyper & Adelman \(2017\)](#))

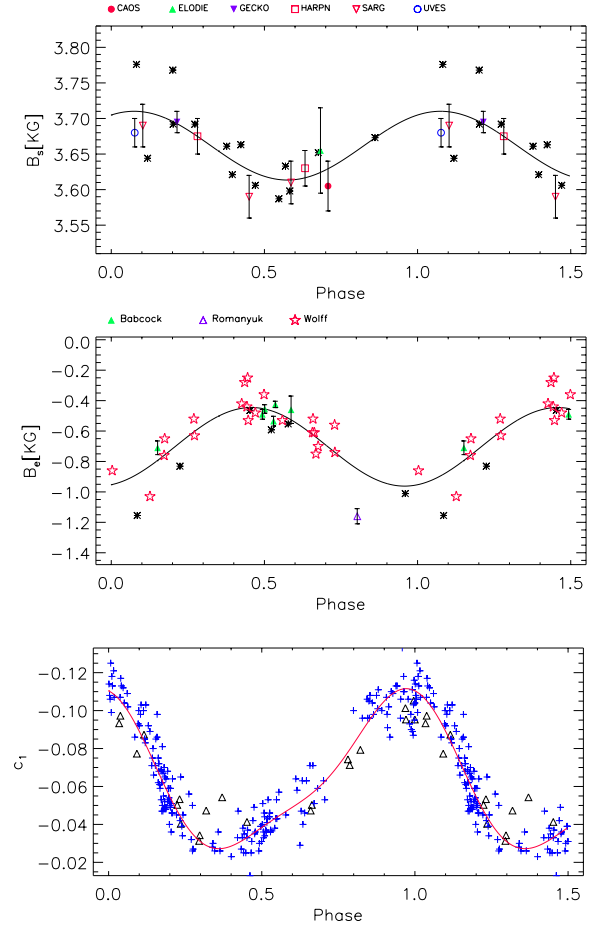


Figure 3. HD 2453. Variation of B_s , B_e and c_1 index by [Wolff \(1975\)](#) (+) and [Pyper & Adelman \(2017\)](#) (Δ).

measurements produce an $L(B_s, B_e, c_1)$ peaking at 517.7 ± 1.8 days. We have then assumed the P17 period to fold the B_s , B_e and c_1 measurements (Fig. 3).

With this period, B_s presents a single wave variation that is in phase with the light curve and with a maximum in coincidence with the negative B_e extremum. This is expected for a dominant dipole component of magnetic field.

3.3 HD 9996

From B_e measurements, [Metlova et al. \(2014\)](#); [Bychkov et al. \(2019\)](#) concluded that the variability period of HD 9996 is 7936.522 days (~ 21.7 yr). [Pyper & Adelman \(2017\)](#) determined the photometric value of 7850 days. M17 assumed the 7936.522 day period resulting in an incomplete phase coverage with B_s maximum coincident in phase with the B_e minimum. Even if folded B_s values were larger than 4000 G, M17 reported of a unsplit FeII 6149.258 Å line in the spectrum of HD 9996 obtained on JD = 2 450 797.312.

We have observed HD 9996 between 2001 and 2021, in addition, we have retrieved two GECKO spectra, one obtained in 2000, from the CFHT archive. Our B_s measurements of HD 9996 are listed in Table 6. We find the variability period given by P17 is representative of the B_s and B_e variations of HD 9996 (Figure 4) with a well-defined maximum and a rather flat minimum. This is not rare for this class of stars (see HD 318107 or HD 335238 later in

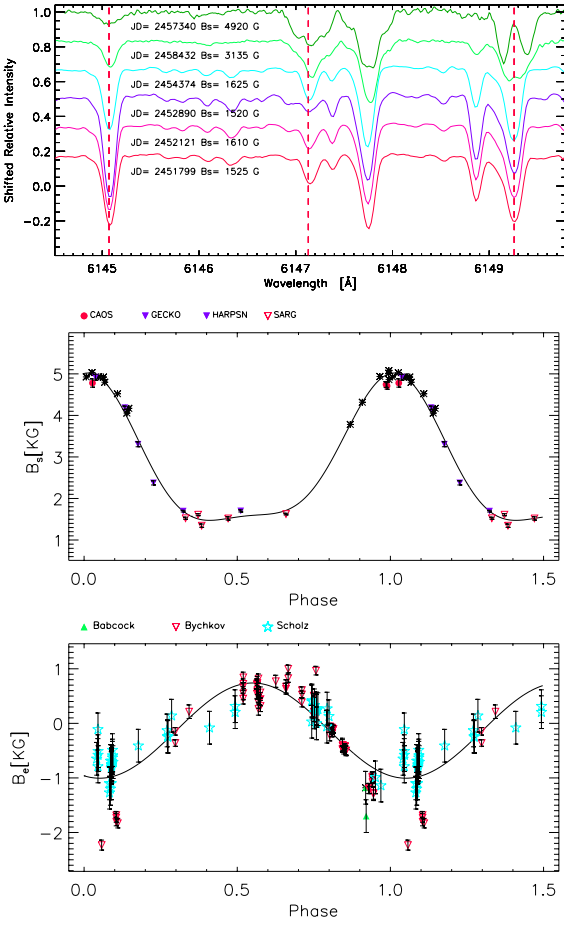


Figure 4. HD 9996. Top, chunk of spectra with marked FeII 6149.258 Å line, the CrII 6147.154 Å line and NdIII 6145.070 Å lines. Normalized spectra are arbitrary shifted for decreasing value of B_s . Cr (6147Å) and Nd (6145Å) abundances change out of phase. Central and lower panels show the B_s and B_e variability.

the text), although it could be that the observed plateau is a consequence of the difficulty in measuring such a weak B_s field because of the merging of Zeeman subcomponents of the FeII 6149.258 Å line (see in Figure 4). Near-infrared lines, that are more sensitive because of the λ^2 Zeeman-split dependence (Leone et al. 2003), should be preferred to determine the real minimum of the B_s variation of HD 9996.

Figure 4 also shows some of these spectra ordered in time and it confirms Preston & Wolff (1970) finding that the equivalent width of chromium and rare-earths spectral lines change out of phase. B_s maximum is coincident with the negative extremum of B_e , while from phase 0.3 to 0.7 B_e presents a maximum and B_s is constant at its minimum value. If the flat minimum is real, HD 9996 presents a magnetic field not purely dipolar.

3.4 HD 12288

Bernhard et al. (2020) found that HD 12288 is a photometric variable with the ephemeris $JD(V^{\max}) = 2457218.6 + 35.73 \pm 0.03$ E days and presenting a peak-to-peak difference equal to 0.02 magnitudes. According to P17, this star is variable in the Strömgren u , v and b filter with the 34.99 day period, but it presents a constant

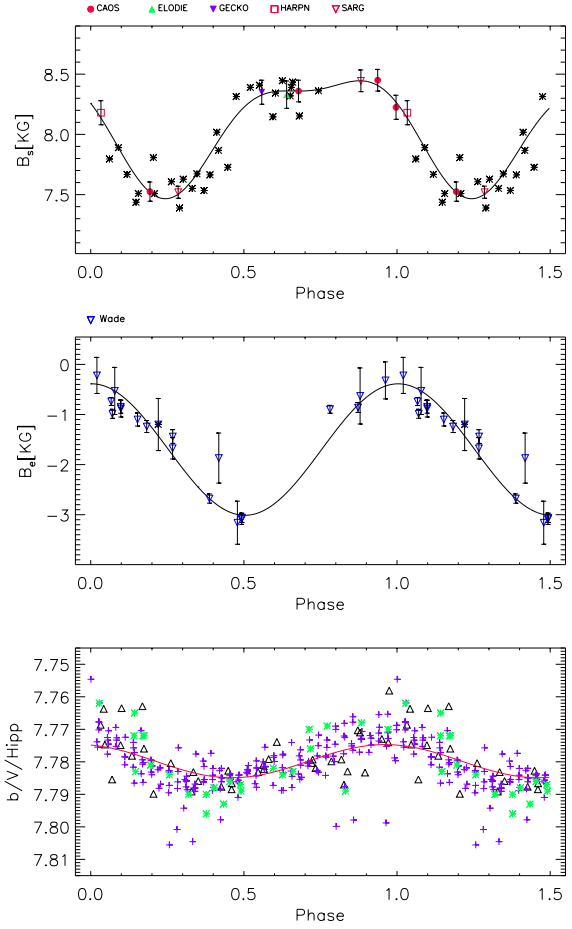


Figure 5. HD 12288

Figure 6. HD 12288. Variability of B_s , B_e by Wade et al. (2000b) and photometry by Wolff & Morrison (1973) (*), HIPPARCOS (Δ) and MAS-CARA (+).

Strömgren y magnitude. A period of 34.9 days was adopted by M17 to discuss the magnetic variability of HD 12288.

We have observed HD 12288 eight times and obtained one spectrum from the ELODIE archive and one from the CFHT one. Consistently with P17, we found the TESS (600-1000 nm) magnitudes obtained from 2458790 to 2458841 constant (7.63688 ± 0.00006). Lomb-Scargle analysis of our (Table 7), M97 and M17 B_s measurements simultaneously to the Wade et al. (2000b) B_e and photometry by Wolff & Morrison (1973), MAS-CARA (Talens et al. 2017; Bernhard et al. 2020), and HIPPARCOS (van Leeuwen 2007) gives the highest peak of $L(B_s, B_e, Mag.)$ at 34.993 ± 0.003 days. Data are folded in Fig. 6. It seems that HD 12288 presents a singular behavior among MCP stars: B_s is almost constant (at the maximum value of 8.5 kG) along half of the rotation period when B_e changes from -3 kG value to zero. And, B_s decreases to 7.5 kG when B_e goes again to -3 kG. This star is brighter when B_e is null.

3.5 HD 14437

The variability period of HD 14437 was determined equal to 26.87 ± 0.02 days by Wade et al. (2000b) from B_e measurements.

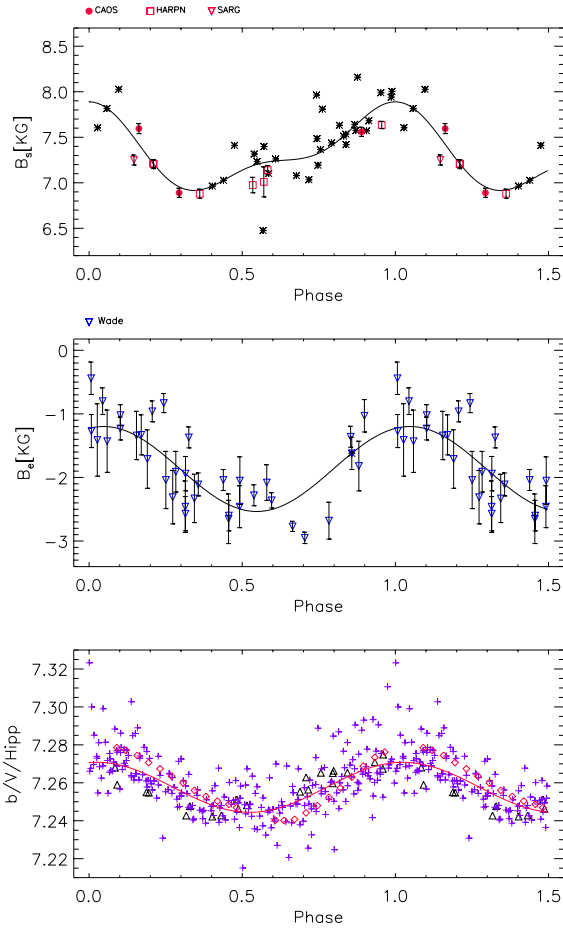


Figure 7. HD 14437. Variability of B_s , B_e by Wade et al. (2000b) and photometry by HIPPARCOS (Δ), TESS (\diamond), and MASCARA (+).

From MASCARA data, Bernhard et al. (2020) found a photometric period of 26.78 ± 0.01 days.

M97 and M17 B_s measurements cover from 1991 to 1997, while our 11 spectra were obtained from 2001 to 2021. We performed a Lomb-Scargle analysis of our (Table 8), M97 and M17 B_s measurements simultaneously to the Wade et al. (2000b) B_e measurements and photometry by HIPPARCOS, TESS, and MASCARA. It results that the period reproducing at the best all variations is 26.734 ± 0.007 days (Fig. 7). B_e presents a single wave variability, while a B_s a double-wave variation cannot be ruled out. The light variability is in phase with the B_s modulation and the magnetic equator is the brightest region (as it is in the case of HD 12288).

3.6 HD 18078

From B_s and B_e measurements, the variability period of HD 18078 has been determined by Mathys et al. (2016b) as long as 1358 ± 12 days.

We have obtained high-resolution spectra of HD 18078 from 2003 up to 2021 with the SARG, CAOS, and HARPS-N. Adopting the previous Mathys et al. (2016b) period our B_s measurements (Table 9) are slightly in advance. A simultaneous Lomb-Scargle analysis gives $L(B_s, B_e)$ with the main peak at 1352 ± 7 days. HIPPARCOS and Strömgren y (Mathys et al. 2016b) photometry are also shown in Fig. 8.

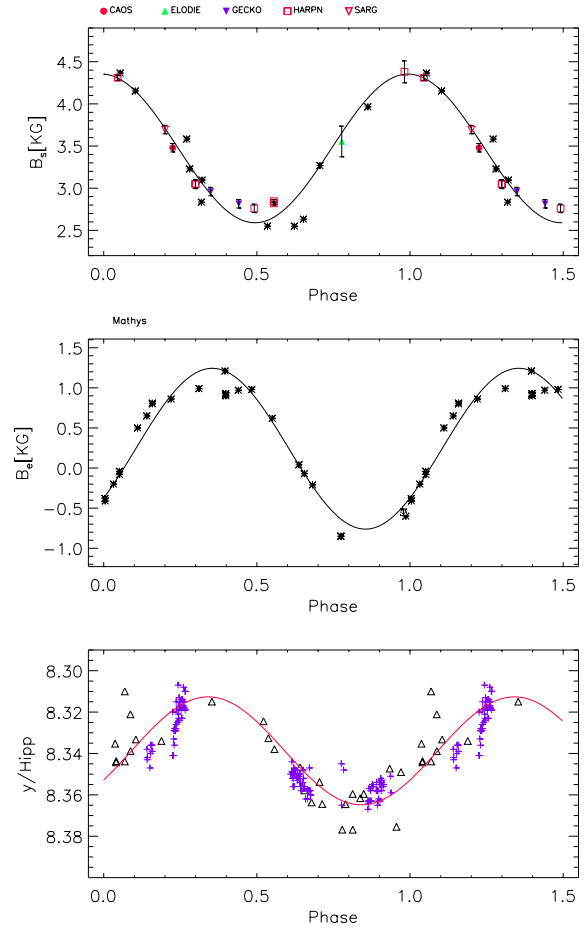


Figure 8. HD 18078. Variability of B_s , B_e by Mathys et al. (2016b) and photometry by HIPPARCOS (Δ) and Mathys et al. (2016b) (+).

3.7 HD 29578

From spectra collected between JD = 2449298 and 2451084 (~ 1786 days), M17 found that the surface magnetic field of HD 29578 changes with a period much longer than 1800 days.

We have obtained one spectrum of HD 29578 with UCLES at the AAT on JD = 2457056.992, unfortunately the FeII 6149.258 Å line region was not included. From other lines the surface magnetic field was estimated as large as ~ 2900 G. We have also obtained from ESO archive one UVES and two FEROS spectra. These B_s measurements (Table 10), plus the ones by M97, M17 and Ryabchikova et al. (2004) extend the time-frame of magnetic measurements to 7759 days.

We have performed a Lomb-Scargle analysis of all available B_s measurements and found in the periodogram two comparable peaks at 4000 and 9230 days (Table 3). Fig. 9 shows the B_s and the B_e (M17) measurements folded with both periods. It appears that new measurements are necessary to determine the period of HD 29578.

Fig. 10 shows the variation of the HD 29578 spectrum in time, from JD = 2451946 (when Zeeman subcomponents are clearly visible) to 2457056, when these overlap. Again, NIR high-resolution spectroscopy seems to be advantageous to define the B_s variability of HD 29578.

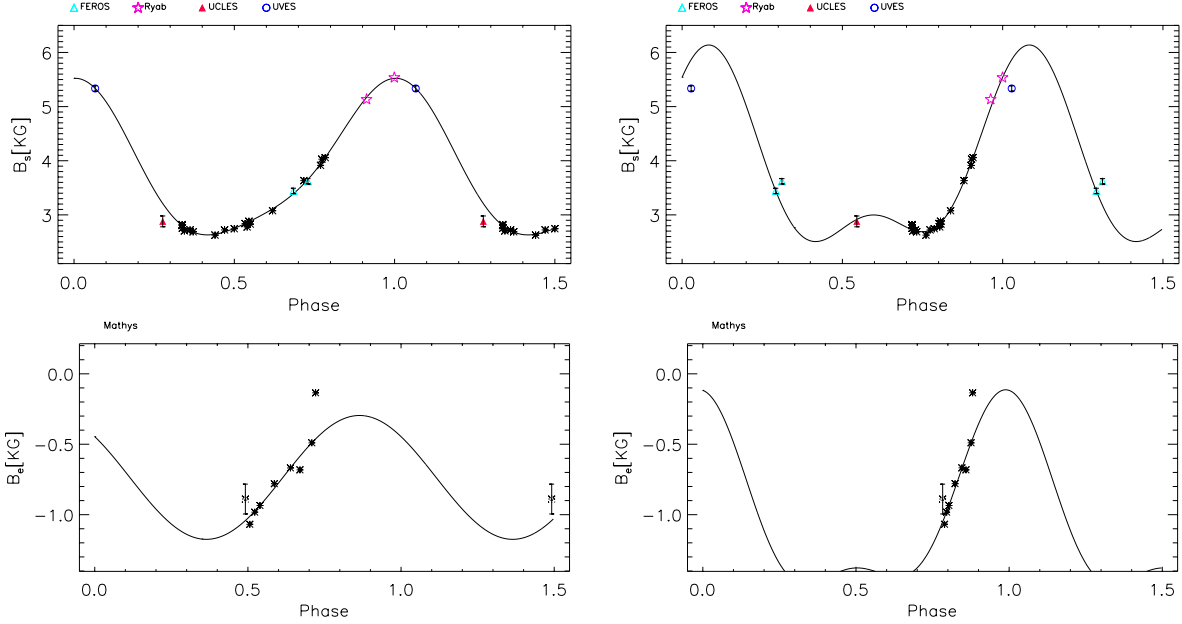


Figure 9. HD 29578. Variability of B_s and B_e by Ryabchikova et al. (2004) (\star) symbols. Left panels show the folding with $P = 4000$ days. Right panels with $P = 9370$ days.

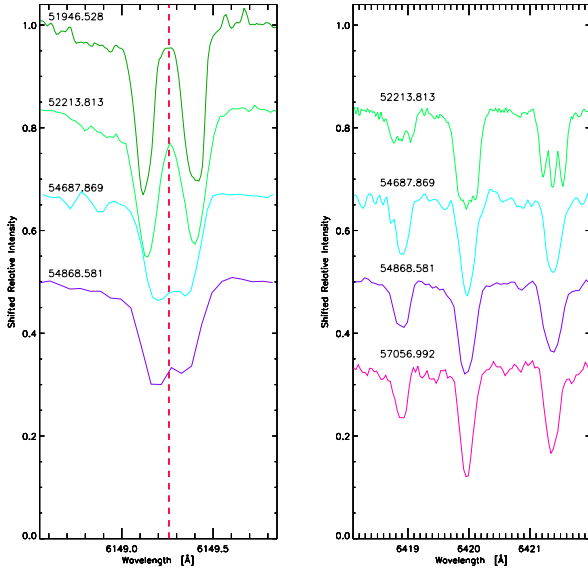


Figure 10. HD 29578. Chunks of spectra ordered for decreasing B_s values. The JD - 2 400 000 is reported. The CES@3.6m-ESO spectrum (JD = 2 451 946.528) goes from 6120 to 6150 Å UCLES@AAT spectrum (JD = 2 457 056.992) does not include the FeII 6149.258 Å line. Zeeman split of other metal lines gives a surface magnetic field of about 2800 G.

3.8 HD 47103

From B_s measurements, obtained between JD = 2449816 and 2451085, M17 found HD 47103 be variable with an extremely long period.

Our measurements of B_s (Table 11) extend the time baseline to 7600 days. We have computed the Lomb-Scargle periodogram $LS(B_s)$ of the B_s measurements, here measured and from literature (Babel & North 1997; Mathys 2017), and the Lomb-Scargle

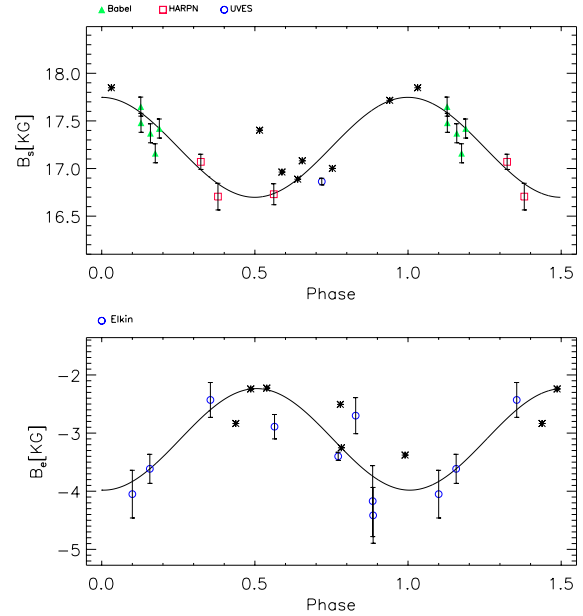


Figure 11. HD 47103. B_s and B_e measurements folded with the period of 17.683 days. Circles are by Elkin & Wade (1997).

periodogram of the B_e measurements by Elkin & Wade (1997) and M17. Hence, $LS(B_s, B_e)$ peaks at 17.683 ± 0.004 days. Fig. 11 presents the B_s and B_e variability.

3.9 HD 50169

Mathys et al. (2019a) found the B_e variability period of HD 50169 equal to 10600 ± 300 days. This value is also representative of their measurements of the surface magnetic field, however covering only 9856 days, which is an interval shorter than a full rotation cycle.

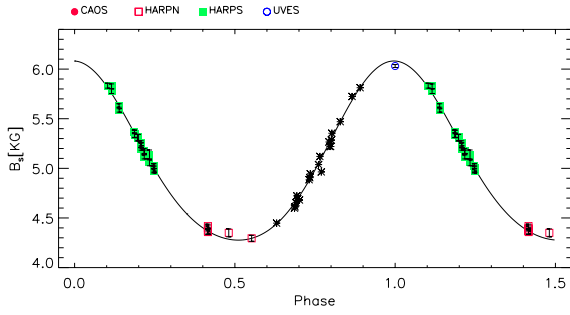


Figure 12. HD50169.

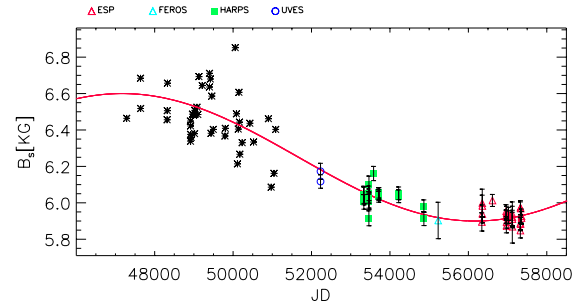


Figure 14. HD55719.

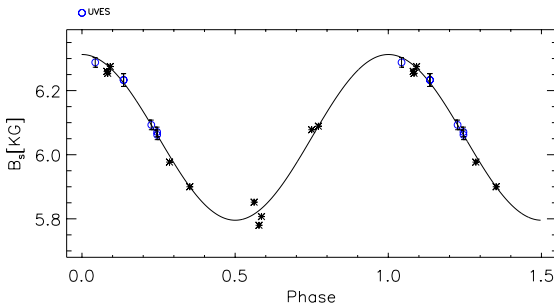


Figure 13. HD51684.

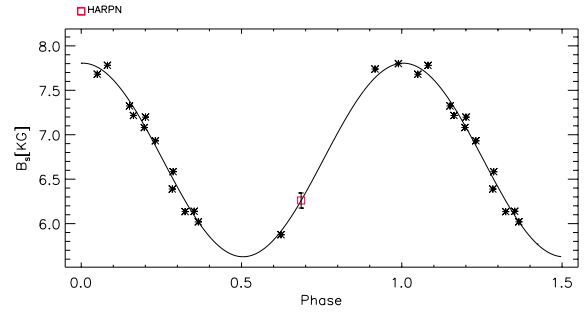


Figure 15. HD61468.

Our B_s measurements (Table 12) slightly extend the time-frame to 10100 days. However, these data confirm the Mathys et al. (2019a) period and establish the shape of the minimum of the B_s variability. The previous uncertainty of 300 days is based on the B_e measurements and it cannot be reduced here. Data are folded in Fig. 12 with the ephemeris given in Table 3.

3.10 HD 51684

From ten measurements of B_s collected between JD = 2450162 and 2451086, M17 concluded that the variability period of HD 51684 is 371 ± 6 days.

In the ESO archive, we found 5 additional UVES spectra spread in 330 days. A Lomb-Scargle analysis of Mathys and our (Table 13) measurements gives a slightly shorter variability period: 366 ± 1 days. Data are folded in Fig. 13.

3.11 HD 55719

M17 analyzed the B_s measurements, collected from JD = 2447285 to 2451086, and found the rotational period of HD 55719 being much longer than ten years.

Our (Table 14) and literature measurements of B_s cover more than 10000 days. We find the surface magnetic field of HD 55719 was always decreasing in the last 27 years, with a rotation period not shorter than 14000 days (38 years) by assuming a simple sinusoidal variation (Fig. 14).

3.12 HD 61468

M17 found the B_s of HD 61468 variable with the 322 ± 3 day period. We have obtained a spectrum of this star with HARPS-North

on JD = 2457340.717 and measured a value for the surface magnetic field $B_s = 6260 \pm 85$ G. A Lomb-Scargle periodogram of M17 and our B_s values presents two merged peaks centered at 321 and 325.5 days. A sine fit of data is in favor of a variability period equal to 321 ± 1 days. Fig. 15 shows the periodic variability of the surface field of HD 61468 with the ephemeris given in Table 3.

3.13 HD 75445

M17 found HD 75445 to be a small amplitude B_s variable with a period of 6.291 days.

Our measurements (Table 16) combined with the surface magnetic field values by M17 and Ryabchikova et al. (2004) span the JD = 2449457 - 2454205 day (~ 13 yr) interval and give an average value of $\langle B_s \rangle = 2970 \pm 55$ G. Lomb-Scargle analysis results in a large number of comparable peaks, with the highest three are at 2.5026, 3.2926 and 6.5500 days.

The constant magnitude (6.9000 ± 0.0003) measured with TESS along 50 days (JD = 2458517 - 2458568), together with the previous B_s r.m.s. (comparable to the measurement error) suggest that, if any, the variability period of HD 75445 is much longer than 13 years (Fig. 16).

3.14 HD 81009

From B_s and B_e measurements, Wade et al. (2000c) determined the variability period of HD 81009 equal to 33.984 ± 0.055 days.

P17 concluded that the photometric variability period of this star is 33.987 ± 0.002 .

Our B_s measurements (Table 17) extend the time coverage of B_s from 1954 days to 8210 days. A Lomb-Scargle analysis of the B_s data confirms the period found by P17. Fig. 17 shows the B_s periodic variability of HD 81009.

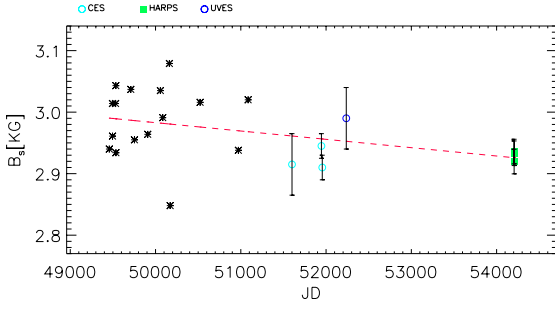


Figure 16. HD75445.

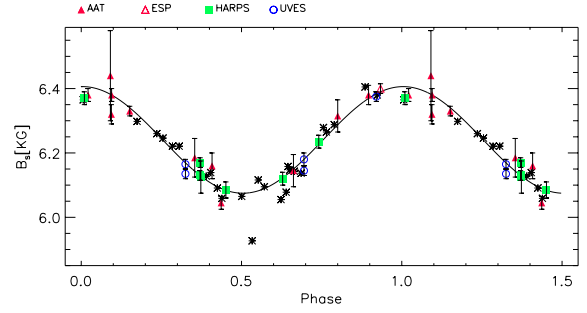


Figure 19. HD94660.

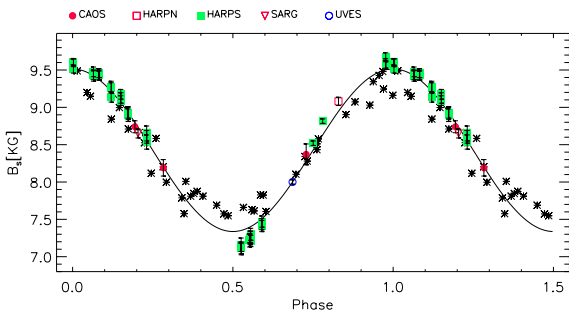


Figure 17. HD81009.

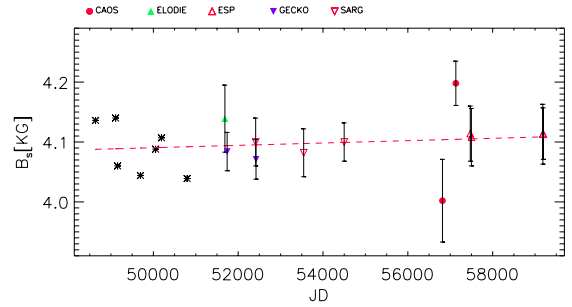
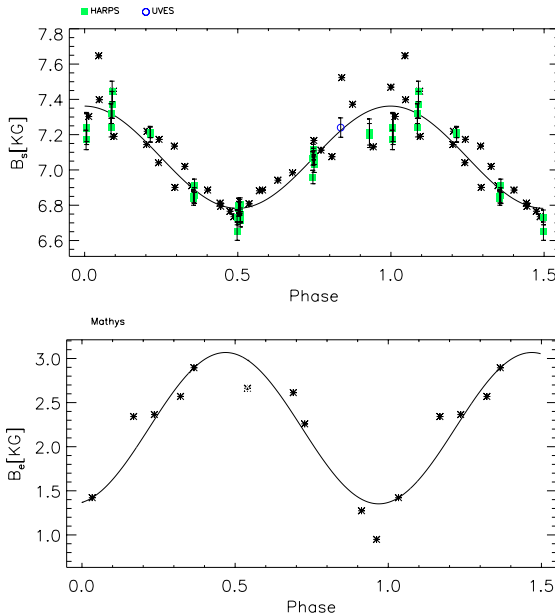


Figure 20. HD110066.


 Figure 18. HD93507. Variability of B_s .

3.15 HD93507

The period of the B_s and B_e variabilities of HD93507 is 556 ± 22 days (M17).

A Lomb-Scargle analysis of B_s measurements by M17, ours (Table 18) and B_e measurements by Mathys (2017) gives a variability period equal to 562 ± 5 day (Fig. 18).

3.16 HD94660

Hensberge (1993) discovered HD94660 be a photometric variable with a period close to 2700 days. From spectra acquired in 12 different nights between May 2001 and April 2014, Bailey et al. (2015) found that this star belongs to a binary system with an orbital period of 804 days and that the rotational period is 2800 days.

We have retrieved the ESO and CFHT archive spectra published by Bailey et al. (2015) and 11 high-resolution spectra of HD94660 obtained between January 1998 and December 2009 with UCLES at the AAT. Our B_s measurements are listed in the Table 19. The Lomb-Scargle periodogram peaks at 2832 days. Fig. 19 shows the B_s periodic variability of HD94660.

Radial velocities have also been measured and combined with the values given by Bailey et al. (2015) to determine the orbital parameters following Catanzaro et al. (2016). Orbital parameters of HD94660, period P_{Orb} , periastron passage date T_0 , orbit eccentricity e , angular anomaly ω , amplitude of radial velocity variation K and system velocity γ , are:

P_{Orb} .	849.1 ± 0.7	d
T_0	$2\,452\,418.2 \pm 1.9$	JD
e	0.43 ± 0.03	
ω	263.5 ± 1.2	$^\circ$
K	17.9 ± 0.5	km s^{-1}
γ	18.4 ± 0.3	km s^{-1}

3.17 HD110066

Pyper & Adelman (2017) reported on a 12-year photometric campaign dedicated to HD110066 without any evidence of variability. M17 found the B_s variability of this star presents an amplitude of 100 G if the period is as long as 4900 days. Bychkov et al. (2020)

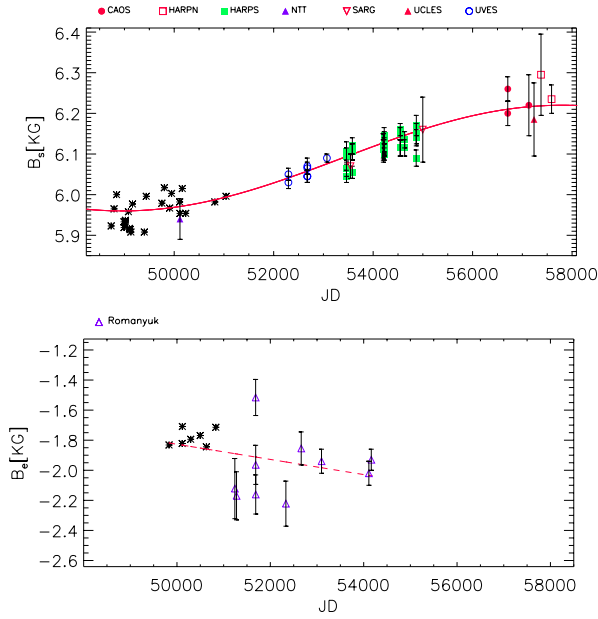


Figure 21. HD 116114. B_s and B_e variability. A sine with the shortest possible period of 17700 days is plotted over the B_s measurements. A linear fit of B_e measurements is also reported.

have obtained new B_e measurements and - considering the positive Babcock's values incorrect - established a variability period of 6.4769 days.

We have analyzed the TESS photometric data and found a constant magnitude (6.346238 ± 0.000003) between JD=2 458 900.0 and 2 458 926.5 (26 days).

Our B_s measurements of HD 110066 are listed in Table 20. Including M97 and M17 values, we span a period of 28.8 years without any evidence of variability. All B_s measurements are between 4040 and 4150 G, with errors not smaller than 50 G. On the basis of B_s measurements, we can only conclude that, if any, the variability period of HD 110066 is longer than three decades, see Fig. 20.

3.18 HD 116114

From measurements collected between JD = 2 448 732 and 2 451 042, M17 found HD 116114 to be a magnetic variable with the 27.61 ± 0.08 day period. The amplitude of the B_s variation is 33 ± 9 G and the amplitude of the B_e variation is equal to 84 ± 33 G. M17 ruled out the 4.41156 day period determined by Romanyuk et al. (2014) from B_e .

We have analyzed the TESS data of HD 116114 (from JD = 2 458 570 to 2 458 595), and found a constant magnitude (6.76799 ± 0.00001) in a time scale of 25 days. Our B_s measurements are listed in Table 21. It appears that B_s measurements cover 8855 days when an always increasing field is observed. This defines the shortest possible period of HD 116114 as equal to 48 years (Fig. 21). The B_e measurements by Mathys & Hubrig (1997); Romanyuk et al. (2014); Mathys (2017) do not present a clear trend.

3.19 HD 126515

Leone & Catanzaro (2001) noted the coincidence of extrema of literature light curves of the star HD 126515 if a variability period

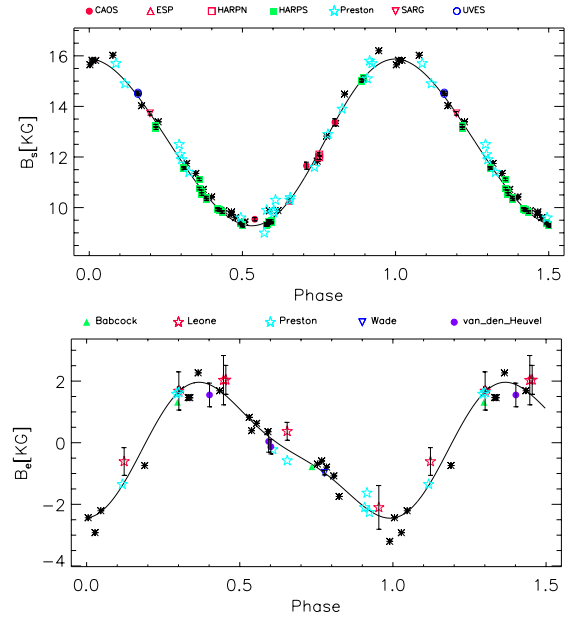


Figure 22. HD 126515. B_s variability. Some of Preston (1970) values (*) are due to Babcock (1958).

equal to 129.9474 days is assumed. This period was also representative of the variability of the B_e and B_s measurements. P17 and M17 established a variability period of 129.95 ± 0.02 days from photometric and magnetic measurements respectively.

By adding our B_s measurements (Table 22) to the literature data by Preston (1970), M97 and M17 we span a total of 23250 days. A Lomb-Scargle analysis of these measurements confirms the validity of the 129.95 day period. Fig. 22 shows the B_s variability and the variability of B_e measurements by Babcock (1958); van den Heuvel (1971); Mathys et al. (1997); Wade et al. (2000a); Leone & Catanzaro (2001); Mathys (2017).

B_s maximum is in coincidence with the negative B_e extremum, while the B_s minimum appears close in phase with a null value of B_e . This is evidence of the departure of the HD 126515 magnetic field from the dipolar configuration.

3.20 HD 137949

After 14 years of monitoring, no evidence of photometric variability has been observed by P17 in HD 137949. From B_e measurements spanning almost 50 years, M17 concluded that the variability period of HD 137949 is 5195 days. By combining our measurements (Table 23) with data available in the literature, we span 10584 days corresponding to twice the period found by Mathys and coworkers. A Lomb-Scargle analysis of B_s and B_e data does not show any predominant peak in the periodogram.

Fig. 23 shows B_s and B_e in time. Both trends are not against a slight increment that, if real, is indicative of a rotational period much longer than 27 years.

Even if all the spectra of HD 137949 recorded between 2002 and 2018 appear constant with equal red and blue σ components for all species, in the SARG spectra obtained on July 13, 14 and 15 2006 the blue σ components appear much weaker than the red one. This difference is particularly large for chromium spectral lines and only marginal for iron lines. Particularly for chromium lines. We have no idea on the persistence and recursivity of this phenomenon,

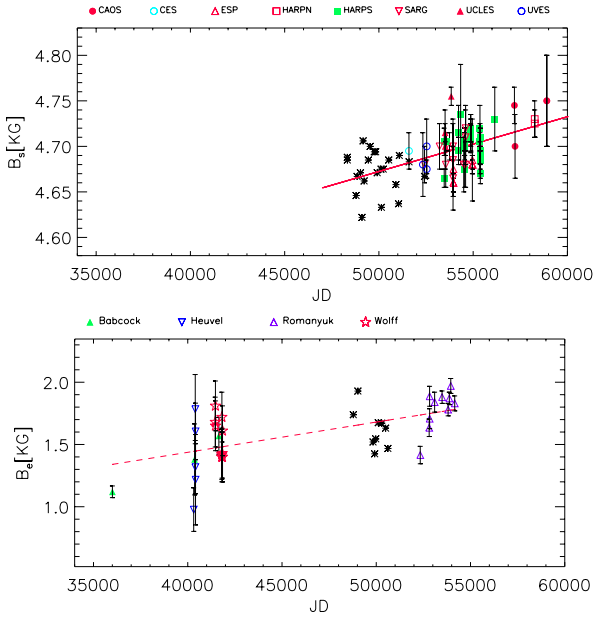


Figure 23. HD 137949. B_s and B_e measurements of in time. The straight lines represent a linear fit of data.

we can only state that it started later than 2006 April 10, and that it ended before August 1, 2006 (Fig. 24). We wonder if such a change is a consequence of a partial occultation of HD 137949 or an occultation of a small size companion across photospheric regions rich in chromium.

3.21 HD 142070

According to Adelman (2001), HD 147010 is a photometric periodic variable with the largest amplitude in the Strömgren v filter and ephemeris: $HJD(v_{min}) = 2450837.499 + 3.37189 \pm 0.00007$ E. M17 found this star is also a magnetic variable with a period of 3.3718 ± 0.0011 days.

Our measurements of B_s are listed in (Table 24). The product $LS(B_s, B_e, v)$ of the periodograms of all available B_s measurements, B_e measurements by M17 and Romanyuk et al. (2014), and Adelman (2001) Strömgren v photometry peaks at 3.3721 ± 0.0002 .

Fig. 25 shows the double wave variation of B_s whose extrema are in phase coincidence with the B_e extrema of HD 142070 with the ephemeris given in Table 3.

3.22 HD 144897

The variability period of the surface magnetic field of HD 144897 was determined by M17 as equal to 48.57 ± 0.15 days from data collected in 7.1 years. To these values, we added our values of B_s (Table 25) for a total range of 22.5 years.

A Lomb-Scargle analysis gives 48.60 ± 0.02 days. Fig. 26 shows all the available measurements of B_s and B_e (Mathys 2017) phased with the ephemeris given in Table 3. Both variations are rather sinusoidal and the B_s minimum in coincidence with the B_e maximum is a proof of a magnetic field far from the dipolar configuration.

3.23 HD 150562

B_s measurements of HD 150562 have been published by M97 and M17 spanning an interval of 4.5 years, Mathys and coworkers concluded that the variability period of this star is longer than 4.5 years.

With our B_s values (Table 26), the coverage is now 21.3 years. Lomb-Scargle analysis of our and Mathys measurements produces a periodogram with the highest peak at 2100 days. Fig. 27 shows the B_s data folded with this period. In the same figure, measurements by Bagnulo et al. (2015) and M17 are too scanty to draw the B_e variability.

At the phase of the maximum, we find an "unexpected" B_s value obtained on JD = 2450171.802 that M17 ascribed to an unidentified cosmic ray. At the same phase, we find another "unexpected" value measured in a HARPS spectrum acquired on JD = 2454338.582. HD 150562 should be observed in 2024 during the next B_s maximum to check if this is the result of chance or to identify a physical reason (e.g. partial occultation of the visible stellar disk by a secondary star).

3.24 HD 154708

The Zeeman components of the FeII 6149.258 Å line of HD 154708 are distant more than 1 Å, meaning that the field in the Zeeman approximation is about 2.4 T, one of the strongest known fields for a non degenerate star. From B_s and B_e measurements, the variability period of HD 154708 has been determined by Hubrig et al. (2009) as equal to 5.3666 ± 0.0007 days. Landstreet et al. (2014) found 5.363 ± 0.003 days.

Here obtained B_s values in the Zeeman approximation are given in Table 27, because of the very strong magnetic field these B_s values are only indicative of the surface magnetic field but, however, representative of the variability. A model of HD 154708 magnetic fields has been published by Stift et al. (2013).

Including in the Lomb-Scargle analysis the B_e by Hubrig et al. (2009) and TESS magnitudes, the highest peak of their product $LS(B_s, B_e, TESS)$ is at 5.367 ± 0.001 days. Fig. 28 shows the variability of TESS photometry, B_e e B_s with the ephemeris given in Table 3. It appears that light variability is driven by the longitudinal component of the field, while a 0.15 phase delay is the B_s variability.

3.25 HDE 318107

As to HDE 318107, the B_s and B_e variability period of 9.7088 ± 0.0007 days was determined by Bailey et al. (2011).

We have obtained 7 HARPS spectra from the ESO archive, 1 GECKO spectrum, and 2 ESPaDOns spectra from the CFHT archive. In addition, we have obtained 1 new spectrum with UCLES and 2 spectra with HARPS-North. Our 13 measurements of B_s (Table 28) have been combined with M17 values for a Lamb-Scargle analysis that peaks at 9.7089 ± 0.0001 days. Fig. 29 shows the B_s and B_e (Mathys & Hubrig (1997), Bagnulo et al. (2015), M17) periodic variability of HDE 318107.

3.26 HD 165474

M97 and M17 present B_s measurements of HD 165474 obtained between 1989 (JD=2447642) and 1998 (JD=2450972) leading to the conclusion that the field is always increasing and the variability period is much longer than nine years. Differently, our B_s measurements between 2004 (JD=2453104) and 2015 (JD=2457229) are

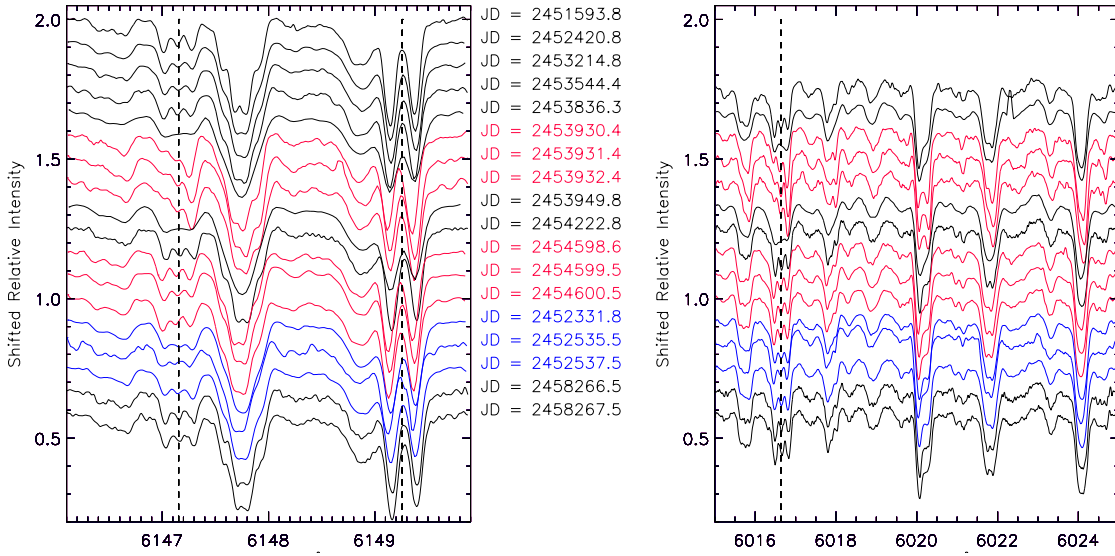


Figure 24. HD 137949. In three consecutive nights, from JD = 2453930 to 245393032 (2006 July 13, 14 and 15) SARG spectra present the red σ Zeeman components deeper than the blue ones, especially for chromium lines. Other series of observations in consecutive days did not show the same behaviour. ESPADONS spectra obtained on JD = 2453 836 and 2453 949 do not show clear Zeeman components because of the reduced resolution as compared to other spectrograph, however they state that the Tthis phenomenon was not longer than 110 days.

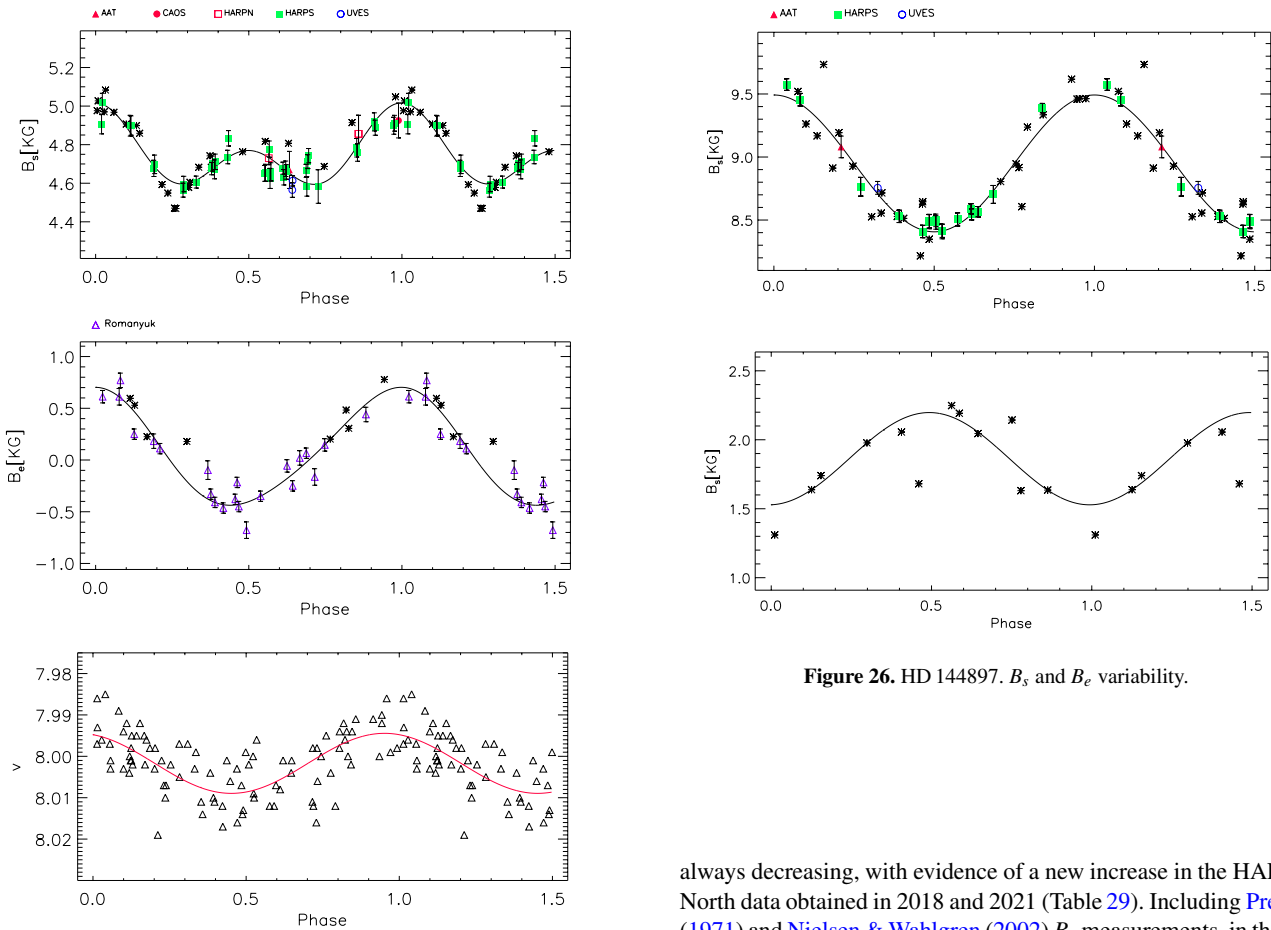


Figure 25. HD 142070. Variability of B_s , B_e (Mathys 2017; Romanyuk et al. 2014) and Strömgren v magnitude.

Figure 26. HD 144897. B_s and B_e variability.

always decreasing, with evidence of a new increase in the HARPS-North data obtained in 2018 and 2021 (Table 29). Including Preston (1971) and Nielsen & Wahlgren (2002) B_s measurements, in the hypothesis of a single harmonic variability, the period is not shorter than 9900 days (27.1 yr): Fig. 30. This value is also compatible with the measurements by Preston (1971) and Nielsen & Wahlgren (2002). As to B_e , data are too scanty for any conclusion.

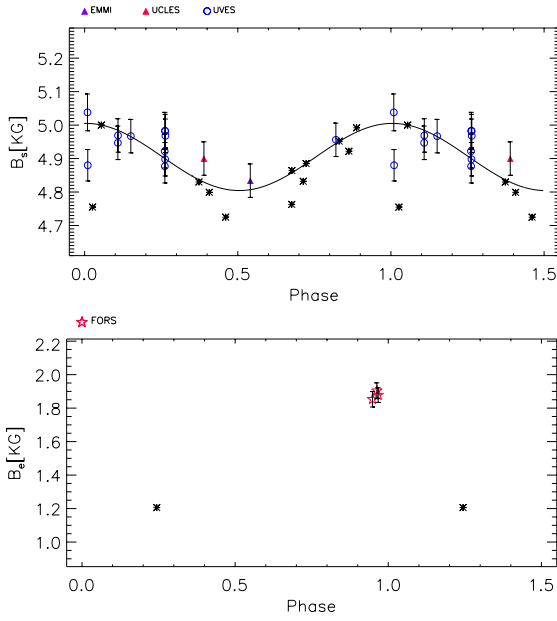


Figure 27. HD 150562. B_s and B_e variability. B_e measurements are by M17 (*) and Bagnulo et al. (2015).

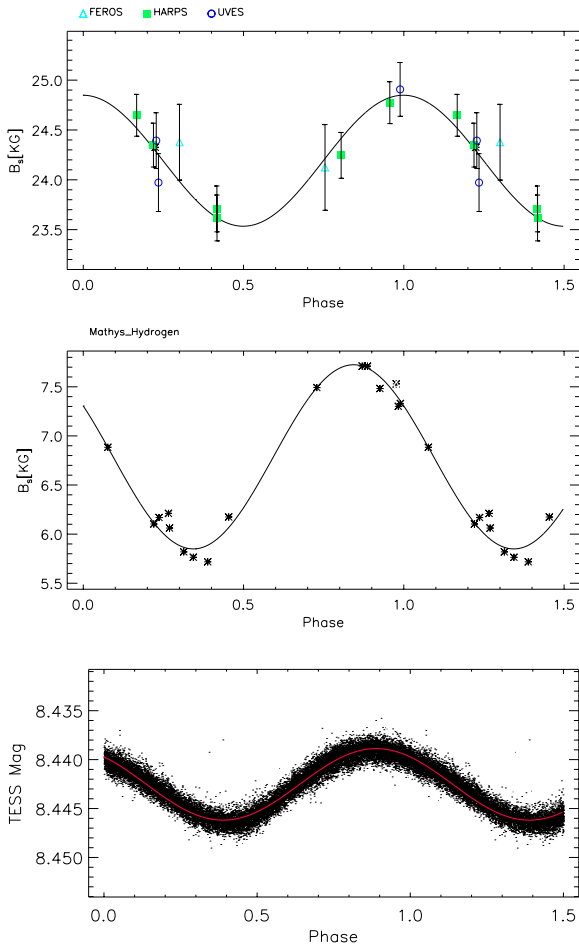


Figure 28. HD 154708. B_s , B_e and TESS photometry variability.

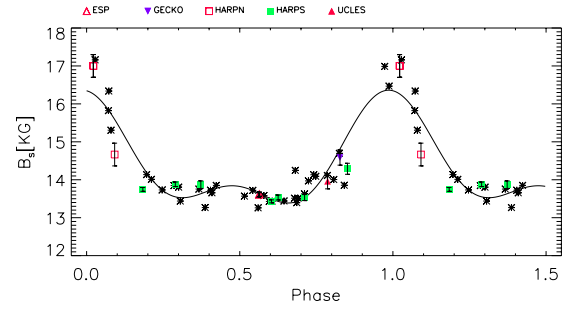


Figure 29. HD318107.

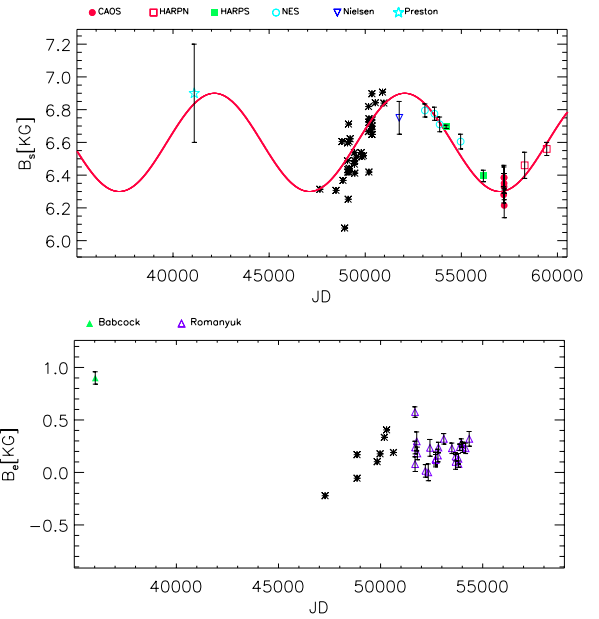


Figure 30. HD165474. B_s and B_e measurements in time. It appears that B_s is variable with a 9900 day period.

3.27 HD 166473

The B_s variability of HD 166473 has been very recently analyzed by Mathys et al. (2020) from spectra also collected from ESO and ESPaDOns archives. These authors determined a period of 3836 days. We have also obtained from ESO and CFHT archive the HD 166473 spectra and add one new measurement: $B_s = 7210 \pm 65$ G, obtained by us with UCLES at the Anglo Australian Telescope on JD = 2 457 235.008. Our measurements (Table 30) confirm this period, and Fig. 31 shows the B_s variability with the ephemeris determined by Mathys and coworkers (Table 3).

3.28 HD 177765

Eight measurements of B_s distributed from 1993 to 1998, plus one literature measurement obtained in 2010, led M17 to the conclusion that the variability period of HD 177765 is longer than 17 years. We have obtained 1 FEROS spectrum and 1 UVES spectrum from the ESO archive and observed HD 177765 once with UCLES and 2 times with HARPS-North. Our B_s measurements (Table 31) extend the temporal baseline from 6 days to almost 25 years and show a continuous increase in time. In the assumption of a simple harmonic variation, the possible shortest period is 37 years (Fig. 32).

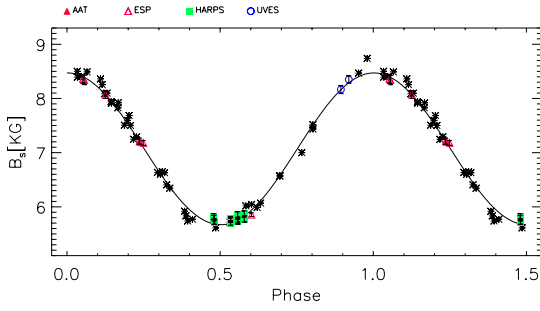


Figure 31. HD166473. B_s variability.

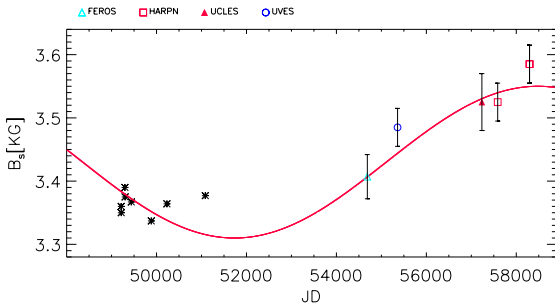


Figure 32. HD 177765. B_s measurements in time.

3.29 HD 178892

From B_e measurements and HIPPARCOS photometry, [Semenko et al. \(2011\)](#) determined the variability period of HD 178892 equal to 8.2549 days.

As to this star, we retrieved 1 HARPS spectrum, 67 UVES spectra obtained from JD = 2455351.334 to JD = 2455351.396 that we have combined in a single spectrum, 1 NES spectrum and 5 ESPaDOs spectra. In addition we have observed this star with HARPS-North two times. Measured values of B_s are in Table 32.

The Lomb-Scargle analysis of our B_s measurements and B_e measurements by [Ryabchikova et al. \(2006\)](#), [Kudryavtsev & Romanyuk \(2012\)](#) and [Romanyuk et al. \(2017\)](#) results in a $L(B_s, B_e)$ with a peak at 8.2572 ± 0.0016 days. Figure 33 shows the folded B_s and B_e variabilities.

3.30 HD 187474

From the B_s measurements collected in the JD = 2447287 - 24551084 (~ 10 yr) interval, M17 established a variability period of 2345 days for HD 187474.

We have acquired high-resolution spectra of HD 187474 two times with UCLES and two times with HARPS, extending the B_s measurements (Table 33) for more than 27 years. We have also observed HD 187474 (see [González et al. 2014](#), for details) with HARPS polarimeter and obtained two measurements of B_e :

HJD	B_e
2456143.760	2125 ± 50 G
2456145.685	2025 ± 50 G

The periodogram of our and M17 B_s measurements and the periodogram of B_e measurements by [Mathys \(1991\)](#), [Mathys & Hubrig \(1997\)](#), M17, [Sikora et al. \(2019\)](#) and us. The $LS(B_s, B_e)$ function

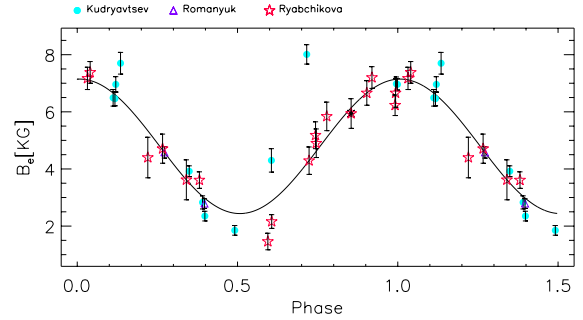
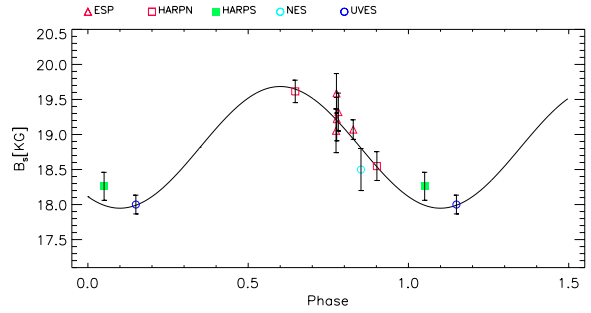


Figure 33. HD 178892: B_s and B_e variability.

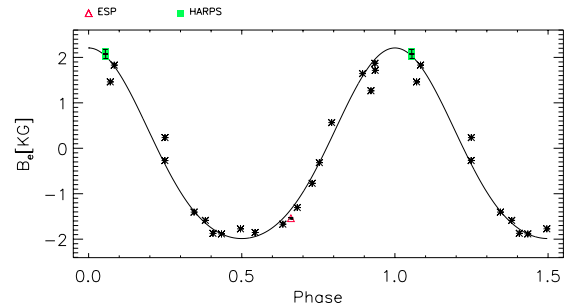
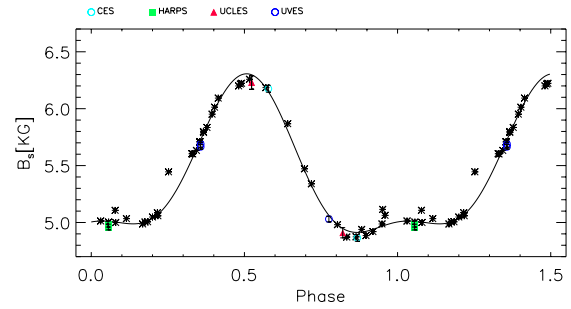


Figure 34. HD 187474. B_s and B_e variability.

peaks at 2329 ± 60 days. Fig. 34 shows the folded B_s and B_e measurements.

An almost constant surface field of 5 kG is measured observing a longitudinal field changing from zero to a 2 kG positive value and then back to zero (variability phase from 0.8 to 1.2). Differently the surface field increases from 5 to 6.3 kG when the negative longitudinal field pass us by (variability phase from 0.2 to 0.8).

3.31 HD 188041

[Mikulášek et al. \(2003\)](#) determined the photometric, magnetic and spectroscopic period of HD 188041 as equal to 223.826 ± 0.040

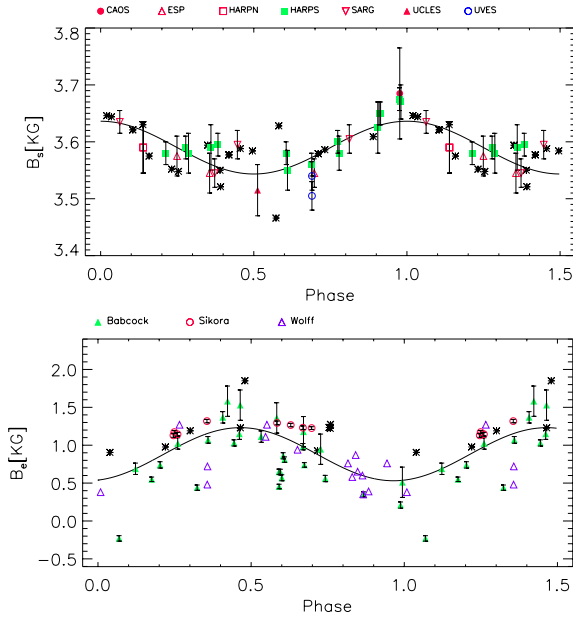


Figure 35. HD 188041. B_s and B_e variability.

days. This period has been adopted by P17 to fold their photometric data. From B_e measurements (covering 50 yr) M17 concluded that this is 223.78 ± 0.10 days.

Our B_s measurements are listed in Table 33 and these extend their time coverage from 2711 (7.4 yr) (Mathys 2017) to 10249 days (28 yr). The literature B_e measurements are by Babcock (1954, 1958), Wolff (1969), Mathys (1991), Mathys et al. (1997), M17, Sikora et al. (2019). So that, $L(B_s, B_e)$ presents a peak at 223.82 ± 0.32 days. The low precision in the period determination is also consequence of the very small amplitude of the B_s variability. In fact, the average value is $\langle B_s \rangle = 3620$ G and the $\sigma = 55$ G is comparable to the typical error in this measurements. Figure 35 shows the B_s and B_e data folded with the Mikulášek et al. (2003) period. It appears that the B_s maximum is in coincidence with the B_e minimum.

3.32 HD 192678

Pyper & Adelman (2017) found the period of 6.4193 days representative of the photometric and magnetic variability shown by HD 192678. The same period was adopted by M17 to discuss the B_s variabilities of this star. However, these authors have also pointed out that the B_e measurements by Wade et al. (1996) do not show any variability with this period. Bychkov et al. (2005) suggested that B_e changes with a period equal to 12.91049 days.

To determine the variability period of HD 192678, we have measured B_s from our and archive spectra (Table 35) and retrieved the TESS photometric data. A Lomb-Scargle analysis of TESS photometry rules out the 12.91049 day period, while $LS(B_s, B_{TESS})$ presents the maximum at 6.4199 ± 0.0001 days, that we have adopted as a period of the HD 192678 variability (Fig. 36). The same figure shows the B_e measurements by Babcock (1958) and Wade et al. (1996) also folded, however still scattered.

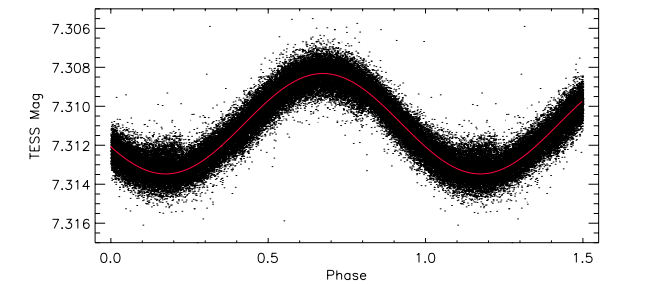
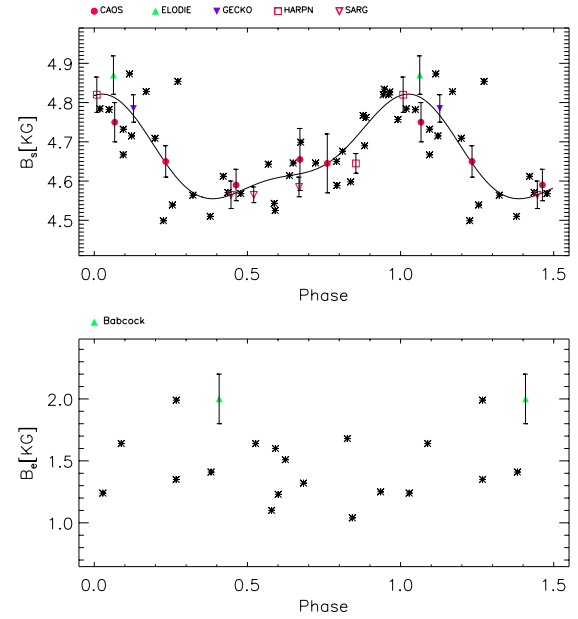


Figure 36. HD 192678. B_s and TESS photometric periodic variability. B_e shows no clear evidence of variability.

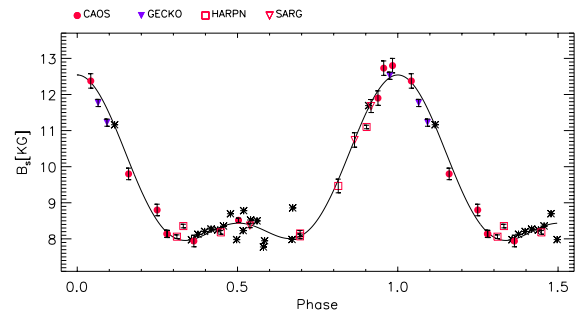


Figure 37. HD HD335238. B_s variability.

3.33 HDE 335238

As to HDE 335238, M17 established a variability period of 48.7 ± 0.1 days from B_s measurements. Most of these data were clustered at the minimum value with only two measurements shaping the B_s maximum.

A Lomb-Scargle analysis of our 22 (Table 36), M97, and M17 measurements produces a periodogram with the highest peak at 48.98 ± 0.02 days. Fig. 37 shows the B_s measurements folded with this period.

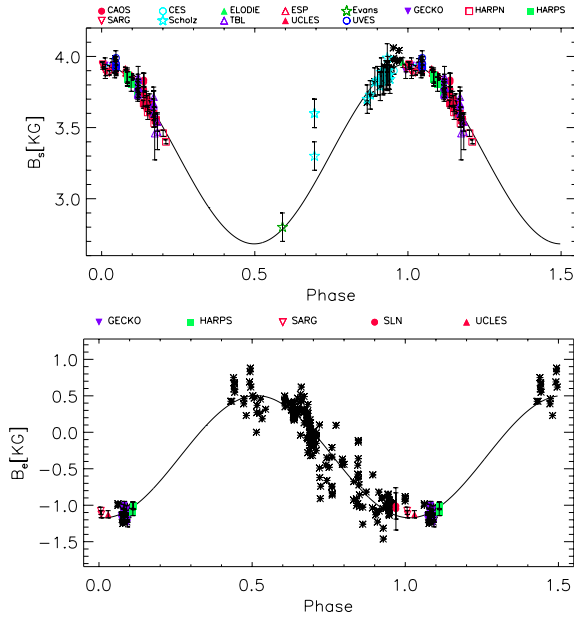


Figure 38. HD 201601. B_s (a) and B_e (b) variability.

3.34 HD 201601

The most recent determination of the variability period of HD 201601 is 97.16 years by [Bychkov et al. \(2016\)](#) under the assumption of a sine variation of B_e .

We have acquired high-resolution spectra of HD 201601 for 24 years with CES (1 spectrum), SARG (8), UCLES (1), HARPS (2), CAOS (14), HARPS (2), and HARPS-North (10). In addition, 58 spectra have been obtained from ESO, CFHT and TBL archives. Measured values of the B_s are listed in Table 37.

To extend as much as possible the time interval of the B_s measurements, we have mined from the available literature and found measurements and estimations also listed in Table 37 with the appropriate references. We have folded with [Bychkov et al. \(2016\)](#) period, these B_s measurements plus the [Evans & Elste \(1971\)](#) and [Scholz \(1979\)](#) values. We find the B_s maximum, on JD = 2 452 200, and a peak-to-peak variation not smaller than 1.3 kG. Among the large numbers of B_e measurements reported in the literature, we here report a sample well distributed in time from the first measurements by [Babcock \(1958\)](#) to present days (Fig. 38). It appears that B_e minimum is coincident with the B_s maximum.

3.35 HD 208217

M17 found the B_s measurements, collected between JD = 2 449 213 and 2 451 085, of HD 208217 variable with the period of 8.44475 days photometrically determined by [Manfroid & Mathys \(1997\)](#). From TESS photometry, [David-Uraz et al. \(2019\)](#) determined a period equal to 8.317 ± 0.001 days.

We have obtained 2 UVES spectra and 8 HARPS spectra from the ESO archive and acquired a new spectrum of HD 208217 with HARPS extending the time coverage to 6932 days. B_s measurements are in Table 38. In addition, we have retrieved the TESS photometric data.

A Lomb-Scargle analysis gives $LS(B_s, B_e, TESS)$ with a peak at 8.445 days (FWHM = 0.005). Figure 39 shows B_s , B_e (M17) and TESS variabilities.

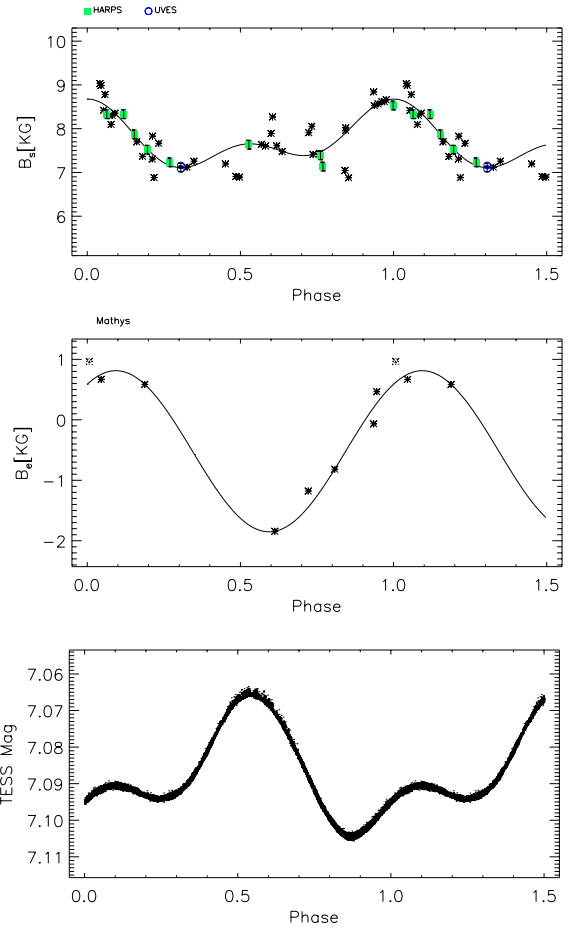


Figure 39. HD 208217. B_s , B_e and TESS-photometry variabilities.

3.36 HD 216018

From spectra collected between 1992 and 1998, M17 concluded that HD 216018 presents, if any, a variability period longer than six years.

Table 39 reports our measurements of B_s from spectra collected from 2001 and 2018. These plus M17 measurements present an average equal to $B_s = 5600 \pm 45$ G. We have computed the Lomb-Scargle periodograms of all B_s data and B_e measurements by M17 and [Romanyuk et al. \(2016\)](#) and found the main peak of $L(B_s, B_e)$ at 34.044 ± 0.007 days. Figure 40 reports the folded B_s and B_e data. Indeed B_s and B_e variabilities presents rather small amplitudes.

4 MAGNETIC FIELD STRENGTH AND ROTATION PERIOD

Figure 41 shows the average surface field versus the rotation period for the here considered stars plus HD 59435, HD 65339, HD 70311, HD 116458 and HD 200311 from M17.

It appears a general decrease of the field with the stellar rotation period. Even if, it is safe to say that the top-right corner is empty, doubts are for the left-bottom corner of Figure 41 being impossible to measure weak surface fields from the distance of the FeII 6149.258 Å Zeeman-components largely broadened by

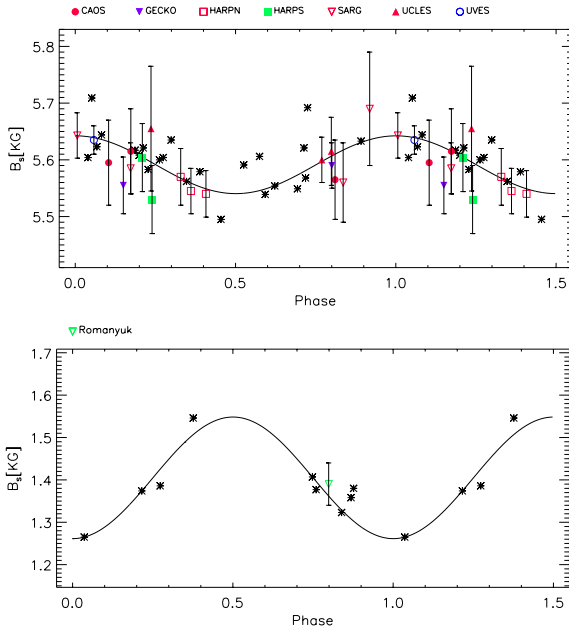


Figure 40. HD 216018. B_s and B_e variability.

the stellar rotation. Thanks to λ^2 dependence of Zeeman-split, a trial could be to look at the near-infrared lines.

The spread for a given value of the period is not justified by the random distribution of angles between the Line-of-Sight, the rotation axis and (if any) the magnetic symmetry axis. For a magnetic dipole, the ratio between the largest and smallest values of B_s is only 1.2 (Preston 1969). Although, in our sample the most extreme case is represented by HD 126515 with a ratio of 1.8. No clear dependence of the field strength appears on temperature or stellar radius.

5 CONCLUSIONS

The surface field of 36 magnetic chemically peculiar stars has been monitored for 20 years. For any star, by adding archive and literature data, we have extended as large as possible the base time with the aim to determine even very long (decades) periods. Fields have been measured from the distance in wavelength of the Zeeman components of FeII 6149.258 Å line in the hypothesis of weak field approximation. For many stars, magnetic fields are so strong that the Paschen-Back effect should be the right approximation for these stars (Stift et al. 2008). The incorrectness of weak field approximation does not affect the determination of the period, but rather the shape of the variability with underestimated amplitudes.

For some stars only the lower limit for the period has been found: HD 55719 with $P > 38$ yr, HD 75445 with $P > 14$ yr, HD 110066 with $P > 29$ yr, HD 116114 with $P > 48$ yr, HD 137949 with $P > 27$ yr, HD 165474 with $P > 27$ yr and HD 177765 with $P > 37$ yr. As to the HD 201601 ($=\gamma$ Equ), the variability period is very close to one century, at the moment the longest established one for this class of stars. We found that the maximum of surface field is coincident with the negative extremum of the longitudinal field.

Figure 41 shows the average surface field versus the here determined rotation periods or the lowest possible value. As a general rule, it appears that stars very long periods show the weakest fields.

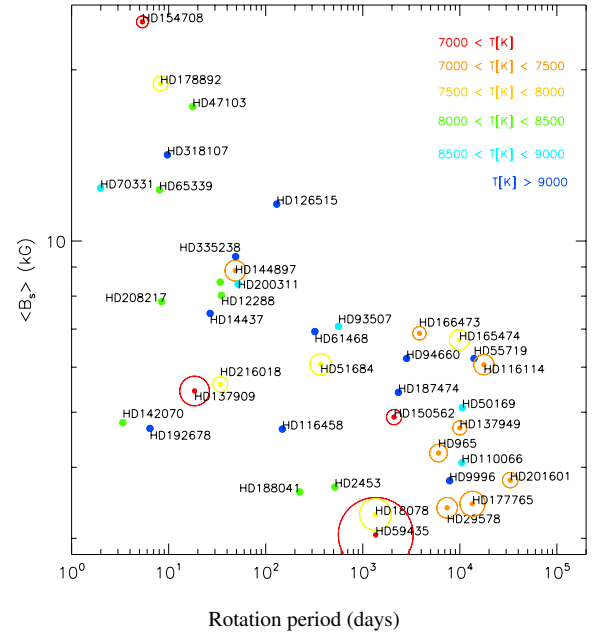


Figure 41. Average surface magnetic field as a function of the rotation period. Colors of filled circles indicate the stellar temperature. If available, GAIA measures of the stellar radius is proportional to the radius of the empty circles. These radii go from 1.66 R_{\odot} (e.g. HD 154708) to 10.47 R_{\odot} (HD 59435).

ACKNOWLEDGMENTS

Based on observations collected at the European Southern Observatory (ESO) and on data obtained from the ESO Science Archive Facility. "Based on observations made with the Italian Telescopio Nazionale Galileo (TNG). The TNG is operated on the island of La Palma by the Fundación Galileo Galilei of the INAF (Istituto Nazionale di Astrofisica) at the Spanish Observatorio del Roque de los Muchachos of the Instituto de Astrofisica de Canarias". This paper includes data collected by the TESS mission. Funding for the TESS mission is provided by the NASA's Science Mission Directorate. This paper includes data collected by the TESS mission, which are publicly available from the Mikulski Archive for Space Telescopes (MAST). Funding for the TESS mission is provided by NASA's Science Mission directorate.

We acknowledge financial contribution from the agreement ASI-INAF n.2018-16-HH.0 and from *Programma ricerca di Ateneo UNICT 2020-22 linea 2*.

REFERENCES

- Adelman S. J., 2001, *A&A*, **368**, 225
 Babcock H. W., 1949, *The Observatory*, **69**, 191
 Babcock H. W., 1954, *ApJ*, **120**, 66
 Babcock H. W., 1958, *ApJS*, **3**, 141
 Babcock H. W., 1960, *ApJ*, **132**, 521
 Babel J., North P., 1997, *A&A*, **325**, 195
 Bagnulo S., Fossati L., Landstreet J. D., Izzo C., 2015, *A&A*, **583**, A115
 Bailey J. D., Landstreet J. D., Bagnulo S., Fossati L., Kochukhov O., Paladini C., Silvester J., Wade G., 2011, *A&A*, **535**, A25
 Bailey J. D., Grunhut J., Landstreet J. D., 2015, *A&A*, **575**, A115
 Baranne A., et al., 1996, *A&AS*, **119**, 373
 Bernhard K., Hümmerich S., Paunzen E., 2020, *MNRAS*, **493**, 3293
 Bychkov V. D., Bychkova L. V., Madej J., 2005, *A&A*, **430**, 1143

- Bychkov V. D., Bychkova L. V., Madej J., 2016, *MNRAS*, **455**, 2567
- Bychkov V. D., Bychkova L. V., Metlova N. V., Madej J., 2019, in Kudryavtsev D. O., Romanyuk I. I., Yakunin I. A., eds, *Astronomical Society of the Pacific Conference Series Vol. 518, Physics of Magnetic Stars*. p. 76
- Bychkov V. D., Bychkova L. V., Madej J., Valiavin G. G., Aitov V. N., 2020, in Romanyuk I. I., Yakunin I. A., Valeev A. F., Kudryavtsev D. O., eds, *Ground-Based Astronomy in Russia. 21st Century*. pp 307–309, doi:10.26119/978-5-6045062-0-2`2020`307
- Catanzaro G., Giarrusso M., Leone F., Munari M., Scalia C., Sparacello E., Scuderi S., 2016, *MNRAS*, **460**, 1999
- Cosentino R., Morales-Juberias R., HDDowling T. E., Butler B. J., 2013, *AGU Fall Meeting Abstracts*, pp P21B–1722
- D’Odorico S., 1990, *The Messenger*, **61**, 51
- David-Uraz A., et al., 2019, *MNRAS*, **487**, 304
- Dekker H., D’Odorico S., Kaufer A., Delabre B., Kotzłowski H., 2000, in Iye M., Moorwood A. F., eds, *Proc. SPIE Vol. 4008, Optical and IR Telescope Instrumentation and Detectors*. pp 534–545, doi:10.1117/12.395512
- Elkin V. G., Wade G. A., 1997, in Glagolevskij Y., Romanyuk I., eds, *Stellar Magnetic Fields*. pp 106–109
- Enard D., 1982, in *Instrumentation in Astronomy IV*. pp 232–242, doi:10.1117/12.933460
- Evans J. C., Elste G., 1971, *A&A*, **12**, 428
- Glaspay J., 1993, *User Manual for GECKO The Coude F/4 Spectrograph*, González J. F., et al., 2014, *A&A*, **561**, A63
- Gratton R. G., et al., 2001, *Experimental Astronomy*, **12**, 107
- Hensberge H., 1993, *Longterm Variability in Cp-Stars*. p. 547
- Horton A., et al., 2012, *CYCLOPS2: the fibre image slicer upgrade for the UCLES high resolution spectrograph*. p. 84463A, doi:10.1117/12.924945
- Hubrig S., Mathys G., Kurtz D. W., Schöller M., Elkin V. G., Henrichs H. F., 2009, *MNRAS*, **396**, 1018
- Kaufer A., Stahl O., Tubbesing S., Nørregaard P., Avila G., Francois P., Pasquini L., Pizzella A., 1999, *The Messenger*, **95**, 8
- Kudryavtsev D. O., Romanyuk I. I., 2012, *Astronomische Nachrichten*, **333**, 41
- Landstreet J. D., Bagnulo S., Fossati L., 2014, *A&A*, **572**, A113
- Leone F., Catanzaro G., 2001, *A&A*, **365**, 118
- Leone F., Vacca W. D., Stift M. J., 2003, *A&A*, **409**, 1055
- Leone F., et al., 2016, *AJ*, **151**, 116
- Leone F., Scalia C., Gangi M., Giarrusso M., Munari M., Scuderi S., Triglio C., Stift M. J., 2017, *ApJ*, **848**, 107
- Manfroid J., Mathys G., 1997, *A&A*, **320**, 497
- Mathys G., 1990, *A&A*, **232**, 151
- Mathys G., 1991, *A&AS*, **89**, 121
- Mathys G., 2017, *A&A*, **601**, A14
- Mathys G., Hubrig S., 1997, *A&AS*, **124**, 475
- Mathys G., Hubrig S., Landstreet J. D., Lanz T., Manfroid J., 1997, *A&AS*, **123**, 353
- Mathys G., Romanyuk I. I., Kudryavtsev D. O., Land street J. D., Pyper D. M., Adelman S. J., 2016a, *A&A*, **586**, A85
- Mathys G., Romanyuk I. I., Kudryavtsev D. O., Land street J. D., Pyper D. M., Adelman S. J., 2016b, *A&A*, **586**, A85
- Mathys G., Romanyuk I. I., Hubrig S., Kudryavtsev D. O., Landstreet J. D., Schöller M., Semenko E. A., Yakunin I. A., 2019a, *A&A*, **624**, A32
- Mathys G., Romanyuk I. I., Hubrig S., Kudryavtsev D. O., Schöller M., Semenko E. A., Yakunin I. A., 2019b, *A&A*, **629**, A39
- Mathys G., Khalack V., Landstreet J. D., 2020, *A&A*, **636**, A6
- Mayor M., et al., 2003, *The Messenger*, **114**, 20
- Metlova N. V., Bychkov V. D., Bychkova L. V., Madej J., 2014, *Astrophysical Bulletin*, **69**, 315
- Mikulášek Z., Žižňovský J., Zverko J., Polosukhina N. S., 2003, *Contributions of the Astronomical Observatory Skalnaté Pleso*, **33**, 29
- Nielsen K., Wahlgren G. M., 2002, *A&A*, **395**, 549
- Panchuk V., Klochkova V., Yushkin M., Naïdenov I., 2009, *J. Opt. Technol.*, **76**, 87
- Press W. H., Rybicki G. B., 1989, *ApJ*, **338**, 277
- Preston G. W., 1969, *ApJ*, **158**, 1081
- Preston G. W., 1970, *ApJ*, **160**, 1059
- Preston G. W., 1971, *ApJ*, **164**, 309
- Preston G. W., Wolff S. C., 1970, *ApJ*, **160**, 1071
- Pyper D. M., Adelman S. J., 2017, *PASP*, **129**, 104203
- Romanyuk I. I., Semenko E. A., Kudryavtsev D. O., 2014, *Astrophysical Bulletin*, **69**, 427
- Romanyuk I. I., Semenko E. A., Kudryavtsev D. O., Moiseeva A. V., 2016, *Astrophysical Bulletin*, **71**, 302
- Romanyuk I. I., Semenko E. A., Kudryavtsev D. O., Moiseeva A. V., Yakunin I. A., 2017, *Astrophysical Bulletin*, **72**, 391
- Ryabchikova T., Nesvacil N., Weiss W. W., Kochukhov O., Stütz C., 2004, *A&A*, **423**, 705
- Ryabchikova T., et al., 2006, *A&A*, **445**, L47
- Scholz G., 1979, *Astronomische Nachrichten*, **300**, 213
- Semenko E. A., Kichigina L. A., Kuchaeva E. Y., 2011, *Astronomische Nachrichten*, **332**, 948
- Sikora J., Wade G. A., Power J., Neiner C., 2019, *MNRAS*, **483**, 3127
- Silvester J., Wade G. A., Kochukhov O., Bagnulo S., Folsom C. P., Hanes D., 2012, *MNRAS*, **426**, 1003
- Stibbs D. W. N., 1950, *MNRAS*, **110**, 395
- Stift M. J., Leone F., Landi Degl’Innocenti E., 2008, *MNRAS*, **385**, 1813
- Stift M. J., Hubrig S., Leone F., Mathys G., 2013, in Shibahashi H., Lynas-Gray A. E., eds, *Astronomical Society of the Pacific Conference Series Vol. 479, Progress in Physics of the Sun and Stars: A New Era in Helio- and Asteroseismology*. p. 125
- Talens G. J. J., Spronck J. F. P., Lesage A. L., Otten G. P. P. L., Stuik R., Pollacco D., Snellen I. A. G., 2017, *A&A*, **601**, A11
- Wade G. A., Elkin V. G., Landstreet J. D., Leroy J. L., Mathys G., Romanyuk I. I., 1996, *A&A*, **313**, 209
- Wade G. A., Donati J. F., Landstreet J. D., Shorlin S. L. S., 2000a, *MNRAS*, **313**, 851
- Wade G. A., Kudryavtsev D., Romanyuk I. I., Land street J. D., Mathys G., 2000b, *A&A*, **355**, 1080
- Wade G. A., Debernardi Y., Mathys G., Bohlender D. A., Hill G. M., Landstreet J. D., 2000c, *A&A*, **361**, 991
- Wolff S. C., 1969, *ApJ*, **158**, 1231
- Wolff S. C., 1975, *ApJ*, **202**, 127
- Wolff S. C., Morrison N. D., 1973, *PASP*, **85**, 141
- Wraight K. T., Fossati L., Netopil M., Paunzen E., Rode-Paunzen M., Bewsher D., Norton A. J., White G. J., 2012, *MNRAS*, **420**, 757
- van Leeuwen F., 2007, *A&A*, **474**, 653
- van den Heuvel E. P. J., 1971, *A&A*, **11**, 461

Table 4. Measured B_s of HD965.

HJD 2400000+	B_s [G]	Sp	HJD 2400000+	B_s [G]	Sp
51691.929	4190 ± 50	US	53715.568	4160 ± 50	HS
51740.091	4250 ± 60	GO	53716.567	4140 ± 50	HS
51741.038	4240 ± 60	GO	54336.860	4120 ± 50	HS
52120.670	4300 ± 40	SG	54338.796	4230 ± 50	HS
52190.627	4280 ± 50	US	54406.585	4230 ± 40	HS
52420.066	4220 ± 40	GO	54442.613	4190 ± 50	HS
52535.699	4290 ± 50	US	54443.560	4090 ± 50	HS
52535.715	4310 ± 50	US	54469.515	4220 ± 50	US
52535.731	4300 ± 50	US	54469.539	4190 ± 50	US
52535.748	4300 ± 50	US	54469.562	4190 ± 50	US
52889.653	4350 ± 40	SG	54469.580	4200 ± 50	US
53270.110	4260 ± 50	UC	56147.773	4200 ± 70	HS
53334.505	4190 ± 50	HS	56648.343	4190 ± 60	HN
53581.741	4110 ± 50	HS	56892.572	4240 ± 110	CS
53582.764	4160 ± 50	HS	56980.341	4260 ± 80	CS
53583.867	4210 ± 50	HS	57252.556	4300 ± 120	CS
53661.707	4110 ± 50	US	57634.482	4270 ± 150	CS
53711.565	4160 ± 50	HS	58367.515	4390 ± 70	CS
53712.595	4150 ± 50	HS	58432.484	4340 ± 50	HN
53713.585	4220 ± 50	HS	58432.495	4300 ± 50	HN
53714.583	4170 ± 50	HS	59441.679	4140 ± 50	HN

Table 5. Measured B_s of HD2453.

HJD 2400000+	B_s [G]	Sp	HJD 2400000+	B_s [G]	Sp
50349.475	3660 ± 60	EE	54374.379	3590 ± 30	SG
52121.649	3690 ± 30	SG	58096.318	3630 ± 30	HN
52890.562	3610 ± 30	SG	58135.220	3610 ± 40	CS
53215.969	3700 ± 20	GO	58432.554	3680 ± 30	CS
53662.628	3680 ± 20	US	59441.749	3670 ± 20	HN

Table 6. Measured surface field of HD9996.

HJD 2400000+	H_s [G]	Sp	HJD 2400000+	H_s [G]	Sp
51740.074	1700 ± 20	GO	56964.449	4710 ± 80	CS
51799.762	1530 ± 30	SG	57264.629	4780 ± 100	CS
52121.660	1610 ± 30	SG	57340.465	4920 ± 70	HN
52212.668	1350 ± 40	SG	58096.461	4190 ± 40	HN
52890.566	1520 ± 40	SG	58432.605	3310 ± 60	HN
53215.113	1700 ± 30	GO	58828.492	2380 ± 50	HN
54374.395	1630 ± 20	SG	59441.695	1680 ± 50	HN
56938.492	4750 ± 70	CS			

Table 7. Measured B_s of HD12288.

HJD 2400000+	B_s [G]	Sp	HJD 2400000+	B_s [G]	Sp
49614.586	8330 ± 110	EE	56964.478	8360 ± 90	CS
52121.691	7520 ± 50	SG	57290.555	8230 ± 100	CS
52212.552	8450 ± 90	SG	57676.762	8180 ± 100	HN
53216.027	8350 ± 100	GO	58137.269	7530 ± 80	CS
56938.528	8450 ± 90	CS	59441.736	8315 ± 50	HN

Table 8. Measured surface field of HD14437.

HJD 2400000+	B_s [G]	Sp	HJD 2400000+	B_s [G]	Sp
52121.719	7250 ± 60	SG	56980.426	7560 ± 50	CS
56651.438	7140 ± 50	HN	58137.293	7600 ± 60	CS
57340.586	6880 ± 50	HN	58432.641	7210 ± 40	HN
57425.414	6980 ± 90	HN	58432.633	7210 ± 50	HN
57426.383	7010 ± 170	HN	59441.723	7640 ± 40	HN
56964.512	6890 ± 50	CS			

Table 9. Measured B_s of HD18078.

HJD 2400000+	B_s [G]	Sp	HJD 2400000+	B_s [G]	Sp
49614.558	3550 ± 180	EE	57340.499	2760 ± 50	HN
51740.120	2960 ± 50	GO	57426.397	2820 ± 20	HN
52890.602	3700 ± 50	SG	57426.408	2850 ± 20	HN
53216.054	2820 ± 50	GO	58432.653	3050 ± 50	HN
56651.484	4380 ± 130	HN	58432.664	3050 ± 50	HN
56980.480	3480 ± 50	CS	59441.708	4310 ± 20	HN

Table 10. Measured B_s of HD29578.

HJD 2400000+	B_s [G]	Sp	HJD 2400000+	B_s [G]	Sp
52213.813	5340 ± 50	US	57056.992	2880 ± 100	UC
54687.869	3440 ± 50	FS	51600.518	5130	(Ry)
54868.581	3620 ± 50	FS	51946.528	5540	(Ry)

Table 11. Measured B_s of HD47103.

HJD 2400000+	B_s [G]	Sp	HJD 2400000+	B_s [G]	Sp
49818.318	17650 ± 100	(B1)	52286.703	16860 ± 40	US
49818.330	17480 ± 100	(B1)	56651.634	16730 ± 110	HN
49819.388	17420 ± 100	(B1)	57425.473	17070 ± 80	HN
50119.485	17370 ± 100	(B1)	57426.463	16710 ± 140	HN
50349.643	17160 ± 100	(B1)			

Table 12. Measured B_s of HD50169.

HJD 2400000+	B_s [G]	Sp	HJD 2400000+	H_s [G]	Sp
52242.612	6030 ± 50	US	54544.631	5180 ± 50	HS
53333.857	5830 ± 50	HS	54545.506	5120 ± 50	HS
53463.496	5780 ± 50	HS	54717.904	5060 ± 50	HS
53464.494	5830 ± 50	HS	54718.910	5140 ± 50	HS
53714.661	5630 ± 50	HS	54865.688	5020 ± 50	HS
53716.633	5590 ± 50	HS	54866.617	4970 ± 50	HS
54222.497	5370 ± 50	HS	54868.697	5000 ± 50	HS
54223.509	5350 ± 50	HS	54869.708	4990 ± 50	HS
54224.523	5330 ± 50	HS	56651.699	4390 ± 50	HN
54336.917	5310 ± 50	HS	56651.665	4420 ± 50	HN
54338.914	5310 ± 50	HS	56651.676	4360 ± 50	HN
54441.674	5230 ± 50	HS	56651.687	4370 ± 50	HN
54442.731	5200 ± 50	HS	57340.620	4350 ± 50	HN
54443.689	5250 ± 50	HS	58075.835	4270 ± 20	US
54443.760	5230 ± 50	HS	58179.551	4270 ± 20	US
54543.493	5160 ± 50	HS	58432.690	4270 ± 50	HN

Table 13. Measured B_s of HD51684.

HJD 2400000+	B_s [G]	Sp	HJD 2400000+	B_s [G]	Sp
53333.817	6090 ± 20	US	53632.847	6290 ± 20	US
53340.802	6070 ± 20	US	53666.765	6230 ± 20	US
53340.816	6060 ± 20	US			

Table 14. Measured B_s of HD55719.

HJD 2400000+	B_s [G]	Sp	HJD 2400000+	B_s [G]	Sp
52229.841	6120 ± 40	US	56353.861	6000 ± 80	ES
52229.841	6170 ± 40	US	56353.865	5980 ± 60	ES
53334.680	6040 ± 50	HS	56613.111	6010 ± 30	ES
53334.681	6040 ± 50	HS	56962.134	5920 ± 40	ES
53334.682	6010 ± 40	HS	56962.144	5950 ± 40	ES
53463.535	6050 ± 40	HS	56968.144	5890 ± 30	ES
53463.536	5920 ± 40	HS	56968.155	5870 ± 40	ES
53463.537	6010 ± 50	HS	56972.106	5940 ± 40	ES
53464.536	6100 ± 50	HS	56972.116	5920 ± 40	ES
53464.538	6010 ± 40	HS	57022.022	5940 ± 40	ES
53464.539	6040 ± 40	HS	57022.032	5920 ± 40	ES
53582.949	6160 ± 40	HS	57120.801	5920 ± 60	ES
53712.674	6030 ± 30	HS	57120.812	5940 ± 70	ES
53712.678	6040 ± 30	HS	57120.823	5910 ± 40	ES
53715.631	6060 ± 30	HS	57120.831	5870 ± 90	ES
53715.636	6050 ± 30	HS	57325.109	5850 ± 40	ES
54222.581	6040 ± 40	HS	57325.117	5880 ± 40	ES
54222.585	6050 ± 40	HS	57325.128	5890 ± 30	ES
54865.672	5980 ± 30	HS	57328.138	5970 ± 40	ES
54865.677	5910 ± 40	HS	57328.148	5970 ± 40	ES
55229.615	5900 ± 100	FS	57353.089	5920 ± 40	ES
56343.815	5900 ± 50	ES	57353.100	5930 ± 40	ES
56353.857	5940 ± 50	ES			

Table 15. Measured B_s of HD61468.

HJD 2400000+	B_s [G]	Sp	HJD 2400000+	B_s [G]	Sp
57340.717	6260 ± 85	HN			

Table 16. Measured B_s of HD75445.

HJD 2400000+	B_s [G]	Sp	HJD 2400000+	B_s [G]	Sp
51600.623	2920 ± 50	CE	54205.492	2930 ± 20	HS
51945.543	2950 ± 20	CE	54205.546	2920 ± 20	HS
51955.501	2910 ± 20	CE	54205.600	2935 ± 20	HS
52236.838	2990 ± 50	US			

Table 17. Measured B_s of HD81009.

HJD 2400000+	B_s [G]	Sp	HJD 2400000+	B_s [G]	Sp
52237.853	8000 ± 30	US	54635.460	8540 ± 100	HS
53463.579	8520 ± 30	HS	54635.464	8610 ± 90	HS
53464.585	8820 ± 30	HS	54635.467	8650 ± 100	HS
54204.530	7220 ± 90	HS	54864.731	9670 ± 60	HS
54204.562	7250 ± 60	HS	54864.734	9580 ± 70	HS
54204.594	7240 ± 60	HS	54864.737	9580 ± 50	HS
54204.627	7250 ± 90	HS	54865.607	9510 ± 60	HS
54222.569	9460 ± 60	HS	54865.610	9610 ± 50	HS
54222.572	9430 ± 70	HS	54865.613	9600 ± 50	HS
54222.575	9430 ± 60	HS	54867.732	9440 ± 70	HS
54498.604	8650 ± 60	SG	54867.735	9480 ± 70	HS
54543.522	7160 ± 90	HS	54867.739	9420 ± 70	HS
54543.525	7110 ± 90	HS	54869.609	9140 ± 70	HS
54543.528	7110 ± 70	HS	54869.612	9280 ± 80	HS
54544.526	7260 ± 80	HS	54869.616	9260 ± 70	HS
54544.529	7300 ± 80	HS	54870.626	9090 ± 70	HS
54544.532	7210 ± 80	HS	54870.630	9180 ± 70	HS
54545.709	7440 ± 80	HS	54870.633	9130 ± 70	HS
54545.712	7410 ± 80	HS	56707.426	8740 ± 80	CS
54545.715	7470 ± 80	HS	56710.441	8190 ± 110	CS
54633.491	8920 ± 90	HS	56759.570	8370 ± 140	CS
54633.494	8900 ± 90	HS	57340.777	9080 ± 60	CS
54633.498	8930 ± 80	HS			

Table 18. Measured B_s of HD93507.

HJD 2400000+	B_s [G]	Sp	HJD 2400000+	B_s [G]	Sp
52244.849	7240 ± 60	US	54545.554	7200 ± 70	HS
53463.672	7170 ± 60	HS	54545.561	7220 ± 70	HS
53464.662	7240 ± 80	HS	54633.540	7240 ± 50	HS
53464.669	7240 ± 90	HS	54633.547	7320 ± 60	HS
53581.463	7220 ± 30	HS	54635.495	7370 ± 80	HS
53581.471	7200 ± 40	HS	54635.503	7450 ± 60	HS
54222.675	6840 ± 40	HS	54864.763	6650 ± 50	HS
54222.683	6850 ± 40	HS	54864.770	6730 ± 40	HS
54224.700	6860 ± 40	HS	54867.605	6800 ± 40	HS
54224.711	6910 ± 40	HS	54867.612	6780 ± 40	HS
54441.807	7070 ± 40	HS	54869.656	6780 ± 40	HS
54441.815	6960 ± 40	HS	54869.663	6790 ± 40	HS
54442.816	7090 ± 30	HS	54870.646	6720 ± 40	HS
54442.823	7120 ± 30	HS	54870.654	6740 ± 40	HS
54443.816	7070 ± 40	HS	54870.742	6800 ± 40	HS
54443.823	7030 ± 40	HS	54870.750	6750 ± 40	HS

Table 19. Measured B_s of HD94660.

HJD 2400000+	B_s [G]	Sp	HJD 2400000+	B_s [G]	Sp
50824.041	6380 ± 40	UC	54196.964	6320 ± 30	UC
51176.136	6380 ± 20	UC	54198.928	6380 ± 20	UC
51542.171	6330 ± 20	UC	54928.959	6190 ± 60	UC
52031.464	6140 ± 20	US	54975.546	6130 ± 20	HS
52031.466	6170 ± 20	US	54976.536	6170 ± 20	HS
52265.250	6160 ± 40	UC	54982.605	6130 ± 50	HS
53072.664	6150 ± 20	US	55161.232	6050 ± 20	UC
53072.705	6180 ± 20	US	55202.867	6090 ± 30	HS
53707.846	6380 ± 20	US	55701.447	6120 ± 20	HS
53745.174	6400 ± 20	ES	56018.549	6240 ± 20	HS
54188.098	6440 ± 40	UC	56775.604	6370 ± 20	HS

Table 20. Measured B_s of HD110066.

HJD 2400000+	B_s [G]	Sp	HJD 2400000+	B_s [G]	Sp
51686.409	4140 ± 60	EE	56816.402	4000 ± 70	CS
51739.759	4080 ± 30	GO	57131.457	4200 ± 40	CS
52412.498	4100 ± 40	SG	57471.933	4110 ± 50	ES
52419.774	4070 ± 30	GO	57498.902	4110 ± 50	ES
53544.371	4080 ± 40	SG	59183.159	4110 ± 50	ES
54498.670	4100 ± 30	SG	59191.150	4110 ± 40	ES

Table 21. Measured B_s of HD116114.

HJD 2400000+	B_s [G]	Sp	HJD 2400000+	B_s [G]	Sp
50115.761	5940 ± 50	EM	54222.786	6120 ± 20	HS
52296.868	6030 ± 20	US	54223.718	6100 ± 20	HS
52296.870	6050 ± 20	US	54223.722	6110 ± 20	HS
52676.855	6070 ± 20	US	54224.827	6130 ± 30	HS
52676.862	6050 ± 20	US	54224.831	6120 ± 20	HS
52676.866	6070 ± 20	US	54544.591	6120 ± 20	HS
52676.869	6050 ± 20	US	54544.595	6120 ± 20	HS
52676.872	6050 ± 20	US	54545.677	6160 ± 20	HS
53070.761	6090 ± 10	US	54545.681	6150 ± 20	HS
53544.389	6070 ± 30	SG	54633.653	6120 ± 20	HS
53463.725	6100 ± 20	HS	54633.657	6140 ± 20	HS
53463.729	6050 ± 20	HS	54865.822	6140 ± 20	HS
53464.703	6110 ± 30	HS	54865.826	6090 ± 20	HS
53464.707	6070 ± 20	HS	54868.760	6170 ± 30	HS
53581.520	6060 ± 20	HS	54868.764	6150 ± 30	HS
53581.524	6110 ± 20	HS	54998.717	6160 ± 80	SG
53582.544	6120 ± 20	HS	56706.596	6200 ± 30	CS
53582.548	6110 ± 20	HS	56707.567	6260 ± 30	CS
54204.668	6120 ± 30	HS	57131.486	6220 ± 80	CS
54204.724	6120 ± 40	HS	57234.859	6190 ± 90	UC
54204.789	6110 ± 30	HS	57375.286	6300 ± 100	HN
54222.782	6150 ± 20	HS	57587.432	6240 ± 40	HN

Table 22. Measured B_s of HD126515.

HJD 2400000+	B_s [G]	Sp	HJD 2400000+	B_s [G]	Sp
51979.910	14490 ± 50	US	54544.705	15050 ± 50	HS
51979.913	14550 ± 50	US	54544.710	15150 ± 50	HS
53463.772	9340 ± 50	HS	54633.662	9340 ± 50	HS
53463.777	9310 ± 50	HS	54633.667	9320 ± 50	HS
53464.756	9460 ± 50	HS	54635.481	9410 ± 50	HS
53464.761	9400 ± 50	HS	54635.486	9470 ± 50	HS
53544.401	13730 ± 70	SG	54716.476	13240 ± 50	HS
53582.603	9370 ± 50	HS	54716.481	13140 ± 50	HS
53582.608	9430 ± 50	HS	54864.815	11120 ± 50	HS
53583.566	9320 ± 50	HS	54864.820	10750 ± 50	HS
53583.571	9280 ± 50	HS	54865.832	10650 ± 50	HS
54222.818	9950 ± 50	HS	54865.837	10540 ± 50	HS
54222.823	9920 ± 50	HS	54867.823	10330 ± 50	HS
54223.696	9890 ± 50	HS	54867.828	10400 ± 50	HS
54223.701	9920 ± 50	HS	56707.654	9540 ± 70	CS
54224.786	9820 ± 50	HS	56729.579	11660 ± 140	CS
54224.791	9830 ± 50	HS	57131.517	13370 ± 140	CS
54338.495	11540 ± 50	HS	58294.454	12100 ± 70	HN
54338.500	11580 ± 50	HS	58294.447	11990 ± 90	HN
54543.828	15010 ± 50	HS	59191.162	10270 ± 80	ES
54543.833	15030 ± 50	HS			

Table 23. Measured B_s of HD137949.

HJD 2400000+	B_s [G]	Sp	HJD 2400000+	B_s [G]	Sp
51593.835	4700 ± 20	CE	54598.589	4680 ± 30	SG
52331.803	4680 ± 40	US	54599.521	4720 ± 30	SG
52420.829	4680 ± 20	SG	54600.478	4710 ± 30	SG
52535.505	4700 ± 30	US	54867.786	4710 ± 20	HS
52537.509	4680 ± 10	US	54867.791	4710 ± 20	HS
53214.796	4700 ± 30	SG	54869.789	4720 ± 20	HS
53463.817	4670 ± 10	HS	54869.794	4720 ± 20	HS
53464.798	4710 ± 20	HS	54870.862	4710 ± 20	HS
53511.082	4720 ± 30	UC	54870.868	4720 ± 20	HS
53513.126	4700 ± 30	UC	54953.976	4680 ± 10	ES
53544.424	4680 ± 30	SG	54957.878	4690 ± 50	ES
53581.602	4710 ± 10	HS	54962.896	4680 ± 10	ES
53745.190	4700 ± 20	ES	54963.000	4680 ± 10	ES
53836.299	4760 ± 10	UC	55360.557	4720 ± 30	HS
53930.384	4700 ± 30	SG	55361.522	4710 ± 10	HS
53931.389	4690 ± 40	SG	55364.472	4690 ± 20	HS
53932.382	4670 ± 40	SG	55365.500	4690 ± 10	HS
53949.814	4660 ± 10	ES	55368.490	4690 ± 20	HS
53950.739	4680 ± 10	ES	55369.502	4700 ± 30	HS
53951.738	4660 ± 10	ES	55379.483	4670 ± 10	HS
54222.804	4700 ± 20	HS	55382.619	4710 ± 10	HS
54223.702	4720 ± 30	HS	55383.663	4710 ± 10	HS
54336.599	4740 ± 60	HS	56145.514	4730 ± 40	HS
54498.750	4680 ± 30	SG	57189.402	4750 ± 20	CS
54543.859	4710 ± 20	HS	57221.350	4700 ± 40	CS
54544.719	4700 ± 20	HS	58266.543	4730 ± 20	HN
54544.724	4710 ± 20	HS	58267.520	4730 ± 20	HN
54545.764	4680 ± 20	HS	58906.500	4750 ± 50	CS
54545.770	4710 ± 20	HS			

Table 24. Measured B_s of HD142070.

HJD 2400000+	B_s [G]	Sp	HJD 2400000+	B_s [G]	Sp
52331.872	4640 ± 40	US	54336.496	4970 ± 50	HS
52331.875	4680 ± 30	US	54543.716	4850 ± 40	HS
53463.840	4680 ± 30	HS	54543.724	4700 ± 50	HS
53464.825	4750 ± 40	HS	54543.734	4730 ± 50	HS
53464.832	4730 ± 40	HS	54543.867	4750 ± 30	HS
53582.617	4720 ± 40	HS	54543.876	4700 ± 40	HS
53582.625	4720 ± 40	HS	54544.873	4990 ± 50	HS
53583.630	4850 ± 50	HS	54544.882	4960 ± 40	HS
53583.638	4830 ± 50	HS	54545.817	4750 ± 40	HS
54222.731	4750 ± 30	HS	54545.826	4770 ± 50	HS
54222.740	4770 ± 40	HS	54866.834	4740 ± 50	HS
54222.909	4810 ± 40	HS	54866.843	4780 ± 40	HS
54222.918	4900 ± 40	HS	54867.862	4780 ± 40	HS
54223.772	4730 ± 30	HS	54867.871	4810 ± 40	HS
54223.780	4650 ± 50	HS	54869.860	4630 ± 40	HS
54223.905	4650 ± 90	HS	54869.869	4670 ± 40	HS
54224.737	4970 ± 40	HS	57229.330	5000 ± 90	CS
54224.745	4980 ± 40	HS	57234.874	4740 ± 100	UC
54224.892	4980 ± 50	HS	58266.509	4800 ± 30	HN
54224.901	5090 ± 50	HS	58267.497	4930 ± 100	HN
54336.487	4970 ± 50	HS	58267.497	4930 ± 100	HN

Table 25. Measured B_s of HD144897.

HJD 2400000+	B_s [G]	Sp	HJD 2400000+	B_s [G]	Sp
52331.834	8760 ± 50	US	54543.815	9390 ± 40	HS
53463.864	8550 ± 40	HS	54543.820	9390 ± 40	HS
53463.869	8550 ± 40	HS	54633.569	8700 ± 70	HS
53464.863	8570 ± 40	HS	54633.574	8700 ± 70	HS
53464.868	8570 ± 40	HS	54716.503	8530 ± 50	HS
53581.632	9580 ± 50	HS	54716.508	8530 ± 50	HS
53581.637	9580 ± 50	HS	54865.843	8410 ± 50	HS
53583.669	9460 ± 50	HS	54865.848	8410 ± 50	HS
53583.674	9460 ± 50	HS	54866.854	8490 ± 50	HS
54224.653	8760 ± 70	HS	54866.859	8490 ± 60	HS
54224.659	8760 ± 70	HS	54867.850	8500 ± 50	HS
54336.542	8510 ± 50	HS	54867.855	8480 ± 50	HS
54336.549	8510 ± 50	HS	54868.800	8410 ± 60	HS
54338.591	8590 ± 40	HS	54868.805	8410 ± 50	HS
54338.598	8590 ± 40	HS	57234.894	9080 ± 90	UC

Table 26. Measured B_s of HD150562.

HJD 2400000+	B_s [G]	Sp	HJD 2400000+	B_s [G]	Sp
51252.826	4830 ± 50	EM	54865.885	4920 ± 50	HS
53939.497	4960 ± 50	US	54866.873	4880 ± 50	HS
54336.532	5040 ± 60	HS	54867.813	4980 ± 60	HS
54338.582	4880 ± 50	HS	54868.819	4900 ± 50	HS
54544.824	4950 ± 50	HS	54869.819	4980 ± 50	HS
54545.846	4970 ± 50	HS	54870.853	4970 ± 50	HS
54633.744	4970 ± 50	HS	57234.910	4900 ± 50	UC

Table 27. Measured B_s of HD154708.

HJD 2400000+	B_s [G]	Sp	HJD 2400000+	B_s [G]	Sp
53631.580	24330 ± 270	US	54633.582	24770 ± 210	HS
53631.596	24390 ± 280	US	54716.543	23710 ± 230	HS
53631.633	23970 ± 290	US	54868.871	24250 ± 230	HS
53662.508	24910 ± 270	US	54870.814	24650 ± 210	HS
54543.769	24350 ± 220	HS	55021.779	24380 ± 380	FS
54544.833	23620 ± 230	HS	55029.581	24120 ± 430	FS

Table 28. Measured B_s of HD318107.

HJD 2400000+	B_s [G]	Sp	HJD 2400000+	B_s [G]	Sp
53215.872	14590 ± 200	GO	54633.608	14290 ± 150	HS
53463.893	13870 ± 100	HS	54869.845	13750 ± 50	HS
53582.640	13430 ± 40	HS	54870.874	13880 ± 60	HS
53583.688	13530 ± 80	HS	57234.963	13960 ± 200	UC
54223.637	13530 ± 70	HS	57587.444	14670 ± 300	HN
54553.120	13600 ± 60	ES	58295.517	17000 ± 300	HN
54553.150	13620 ± 60	ES	58295.517	17000 ± 300	HN

Table 29. Measured B_s of HD165474.

HJD 2400000+	B_s [G]	Sp	HJD 2400000+	B_s [G]	Sp
53104.452	6800 ± 40	NS	57220.407	6390 ± 70	CS
53601.345	6780 ± 40	NS	57221.375	6390 ± 80	CS
53871.451	6710 ± 50	NS	57222.435	6330 ± 80	CS
54207.848	6700 ± 10	HS	57223.381	6350 ± 60	CS
54963.440	6610 ± 50	NS	57229.452	6220 ± 80	CS
56145.616	6400 ± 40	HS	58294.554	6460 ± 80	HN
57202.477	6280 ± 50	CS	59441.374	6560 ± 40	HN

Table 30. Measured B_s of HD166473.

HJD 2400000+	B_s [G]	Sp	HJD 2400000+	B_s [G]	Sp
52090.459	8170 ± 80	US	54634.852	5730 ± 50	HS
52189.506	8350 ± 70	US	54634.861	5860 ± 50	HS
54336.612	5790 ± 50	HS	54716.623	5770 ± 50	HS
54336.622	5830 ± 50	HS	54716.633	5880 ± 50	HS
54338.630	5720 ± 50	HS	56531.773	8360 ± 80	ES
54338.639	5730 ± 50	HS	56547.732	8340 ± 90	ES
54544.782	5780 ± 40	HS	56813.014	8070 ± 70	ES
54544.791	5760 ± 50	HS	57239.836	7210 ± 50	ES
54545.866	5760 ± 40	HS	57287.712	7180 ± 50	ES
54545.872	5700 ± 40	HS	58642.993	5860 ± 40	ES
54633.767	5760 ± 40	HS	57235.008	7210 ± 70	UC
54633.777	5740 ± 40	HS			

Table 31. Measured B_s of HD177765.

HJD 2400000+	B_s [G]	Sp	HJD 2400000+	B_s [G]	Sp
54687.752	3410 ± 40	FS	57586.569	3530 ± 30	HN
55359.817	3490 ± 30	US	58294.607	3590 ± 30	HN
57235.029	3530 ± 50	UC			

Table 32. Measured B_s of HD178892.

HJD 2400000+	B_s [G]	Sp	HJD 2400000+	B_s [G]	Sp
53871.405	18500 ± 300	NS	53871.405	18500 ± 300	NS
55351.884	18000 ± 140	US	55351.884	18000 ± 140	US
56356.149	19050 ± 310	ES	56356.149	19050 ± 310	ES
56356.160	19590 ± 280	ES	56356.160	19590 ± 280	ES
56356.166	19220 ± 310	ES	56356.166	19220 ± 310	ES
56430.906	19070 ± 140	ES	56430.906	19070 ± 140	ES
56471.808	19320 ± 270	ES	56471.808	19320 ± 270	ES
57587.510	18550 ± 210	HN	57587.510	18550 ± 210	HN
58295.517	19620 ± 160	HN	58295.517	19620 ± 160	HN
53600.561	18260 ± 200	HS			

Table 33. Measured B_s of HD187474.

HJD 2400000+	B_s [G]	Sp	HJD 2400000+	B_s [G]	Sp
50375.159	6180 ± 30	CE	53270.000	4910 ± 50	UC
51051.667	4870 ± 30	CE	56143.760	4990 ± 30	HS
53164.788	5030 ± 30	US	56145.685	4960 ± 30	HS
52189.525	5670 ± 20	US	57235.076	6230 ± 60	UC
52189.526	5690 ± 30	US			

Table 34. Measured B_s of HD188041.

HJD 2400000+	B_s [G]	Sp	HJD 2400000+	B_s [G]	Sp
51826.349	3640 ± 20	SG	54338.672	3580 ± 40	HS
52119.549	3550 ± 30	SG	54374.362	3600 ± 30	SG
52190.600	3510 ± 30	US	54545.899	3580 ± 20	HS
52190.601	3540 ± 30	US	54633.859	3580 ± 20	HS
52889.376	3610 ± 30	SG	54634.808	3550 ± 40	HS
53270.015	3520 ± 50	UC	54716.644	3680 ± 20	HS
53464.884	3600 ± 20	HS	54717.696	3670 ± 30	HS
53581.663	3630 ± 50	HS	56145.652	3590 ± 40	HS
53582.668	3650 ± 20	HS	56507.449	3690 ± 80	CS
53583.716	3650 ± 20	HS	57239.986	3580 ± 40	ES
54204.876	3560 ± 20	HS	57263.823	3550 ± 40	ES
54223.864	3600 ± 20	HS	57564.132	3550 ± 30	ES
54224.862	3580 ± 30	HS	57886.723	3590 ± 50	HN
54336.651	3590 ± 20	HS			

Table 35. Measured B_s of HD192678.

HJD 2400000+	B_s [G]	Sp	HJD 2400000+	B_s [G]	Sp
49620.334	4870 ± 50	EE	57221.522	4750 ± 50	CS
52120.616	4570 ± 20	SG	57222.591	4650 ± 40	CS
52121.564	4590 ± 30	SG	57230.486	4590 ± 40	CS
52890.527	4570 ± 40	SG	57264.497	4650 ± 80	CS
53215.898	4790 ± 40	GO	58266.601	4650 ± 30	HN
56904.409	4660 ± 80	CS	58267.591	4820 ± 50	HN

Table 36. Measured B_s of HD335238.

HJD 2400000+	B_s [G]	Sp	HJD 2400000+	B_s [G]	Sp
51739.542	11770 ± 100	GO	57240.524	7940 ± 160	CS
51740.896	11220 ± 100	GO	57959.548	12380 ± 200	CS
52420.916	12520 ± 100	GO	57611.553	11900 ± 200	CS
52121.622	10740 ± 200	SG	58299.573	12800 ± 200	CS
52889.396	8370 ± 60	SG	58312.588	8800 ± 160	CS
53544.714	11680 ± 180	SG	57587.537	8180 ± 50	HN
56844.590	8140 ± 100	CS	58095.336	9470 ± 190	HN
56893.490	8140 ± 100	CS	58266.621	8060 ± 50	HN
56904.447	8520 ± 60	CS	58267.602	8360 ± 50	HN
57220.548	12730 ± 200	CS	58295.601	11100 ± 50	HN
57230.548	9800 ± 160	CS	58432.375	8070 ± 70	HN

Table 37. Measured B_s of HD201601.

HJD 2400000+	B_s [G]	Sp	HJD 2400000+	B_s [G]	Sp
37476.500	2800 ± 100	Evans	55168.747	3880 ± 20	ES
41180.411	3600 ± 100	Scholz	55406.850	3860 ± 20	ES
41181.410	3300 ± 100	Scholz	55415.600	3810 ± 50	HS
41182.454	3600 ± 100	Scholz	55490.789	3870 ± 20	ES
47283.000	3700 ± 100	Scholz	55517.704	3840 ± 10	ES
47638.000	3730 ± 100	Scholz	55523.729	3860 ± 10	ES
48169.000	3820 ± 100	Scholz	55524.694	3850 ± 20	ES
48479.000	3830 ± 100	Scholz	55530.768	3860 ± 20	ES
48790.000	3790 ± 100	Scholz	56124.801	3810 ± 50	HS
48925.000	3890 ± 100	Scholz	56126.795	3750 ± 50	HS
49102.000	3830 ± 100	Scholz	56148.712	3760 ± 50	HS
49216.000	3840 ± 100	Scholz	56175.495	3730 ± 50	NL
49457.000	3870 ± 100	Scholz	56176.477	3790 ± 40	NL
49577.000	3860 ± 100	Scholz	56182.373	3740 ± 30	NL
49608.000	3990 ± 100	Scholz	56185.408	3790 ± 40	NL
49696.000	3900 ± 100	Scholz	56234.241	3840 ± 40	NL
49829.000	3870 ± 100	Scholz	56238.250	3860 ± 80	NL
49909.000	3840 ± 100	Scholz	56239.237	3780 ± 80	NL
50374.500	3900 ± 30	CE	56251.237	3790 ± 60	NL
51404.518	3960 ± 30	EE	56252.224	3780 ± 40	NL
51740.013	3900 ± 50	GO	56822.587	3670 ± 30	CS
51773.570	3920 ± 30	SG	56829.600	3740 ± 30	CS
52117.649	3940 ± 30	SG	56830.592	3670 ± 30	CS
52118.547	3950 ± 20	SG	56873.544	3670 ± 20	HN
52412.722	3900 ± 50	SG	56881.466	3770 ± 20	CS
52420.042	3940 ± 50	GO	56881.474	3820 ± 60	CS
52463.730	3890 ± 30	SG	56892.403	3840 ± 50	CS
52889.433	3890 ± 20	SG	57180.587	3660 ± 40	CS
52920.569	3920 ± 20	CE	57189.576	3650 ± 20	CS
53214.938	3940 ± 50	GO	57190.580	3650 ± 20	CS
53270.053	3940 ± 20	UC	57192.517	3710 ± 50	CS
53464.922	3930 ± 10	HS	57193.515	3700 ± 30	CS
53508.708	3900 ± 50	SG	57202.542	3640 ± 20	CS
53512.343	3960 ± 50	UC	57235.083	3690 ± 40	UC
53513.268	3940 ± 50	UC	57240.045	3690 ± 40	ES
53515.269	3940 ± 50	UC	57252.503	3670 ± 30	CS
53541.052	3910 ± 20	ES	57340.357	3610 ± 50	HN
53544.690	3940 ± 20	SG	57340.362	3640 ± 30	HN
53581.690	3920 ± 20	HS	57564.136	3670 ± 30	ES
53582.725	3930 ± 10	HS	57575.590	3690 ± 50	CS
53583.743	3920 ± 20	HS	57586.595	3670 ± 20	HN
53631.752	3930 ± 50	US	57587.561	3610 ± 20	HN
53659.599	3990 ± 50	US	57900.725	3590 ± 20	HN
53659.600	3920 ± 50	US	58012.494	3600 ± 30	HN
53659.600	3950 ± 50	US	58036.391	3670 ± 90	NL
53659.601	3930 ± 50	US	58036.392	3600 ± 100	NL
53659.602	3950 ± 50	US	58037.396	3650 ± 110	NL
54753.743	3910 ± 20	ES	58037.397	3720 ± 70	NL
54818.720	3890 ± 20	ES	58060.696	3580 ± 10	ES
54963.124	3880 ± 20	ES	58094.806	3530 ± 30	HN
54975.828	3860 ± 50	HS	58143.240	3460 ± 190	NL
54975.833	3840 ± 50	HS	58266.684	3550 ± 20	HN
54976.828	3850 ± 50	HS	58267.637	3560 ± 40	HN
54976.833	3870 ± 50	HS	58463.222	3470 ± 130	NL
55028.949	3880 ± 20	ES	58464.225	3540 ± 70	NL
55029.049	3880 ± 10	ES	58474.715	3540 ± 20	ES
55110.824	3880 ± 20	ES	59119.381	3460 ± 20	HN
55160.747	3870 ± 20	ES	59441.366	3400 ± 20	HN

Table 38. Measured surface field of HD208217.

HJD 2400000+	B_s [G]	Sp	HJD 2400000+	B_s [G]	Sp
52189.566	7080 ± 60	US	53715.523	8530 ± 100	HS
52189.570	7160 ± 50	US	53716.539	8330 ± 100	HS
53581.711	7870 ± 100	HS	54205.883	8330 ± 100	HS
53582.691	7230 ± 100	HS	54223.891	7520 ± 100	HS
53711.547	7640 ± 100	HS	56145.746	7140 ± 100	HS
53713.520	7390 ± 100	HS			

Table 39. Measured B_s of HD216018.

HJD 2400000+	B_s [G]	Sp	HJD 2400000+	B_s [G]	Sp
52117.670	5690 ± 100	SG	56144.761	5600 ± 60	HS
52120.654	5640 ± 40	SG	56145.791	5530 ± 60	HS
52190.510	5640 ± 30	US	56892.507	5620 ± 80	CS
52420.046	5590 ± 40	GO	57220.589	5570 ± 70	CS
53214.957	5560 ± 50	GO	57230.588	5600 ± 80	CS
53270.083	5600 ± 40	UC	57235.088	5660 ± 110	UC
53271.093	5620 ± 60	UC	57340.376	5570 ± 50	HN
53544.700	5560 ± 70	SG	58294.694	5550 ± 40	HN
53930.653	5590 ± 50	SG	58432.465	5540 ± 40	HN